Host exciton confinement for enhanced Förster-transfer-blend gain media yielding highly efficient yellow-green lasers

Qi Zhang[#] Jingguan Liu, Qi Wei, Xiangru Guo, Yan Xu, Ruidong Xia, Linghai Xie, Yan Qian,* Chen Sun, Larry Lüer, Juan Cabanillas-Gonzalez,* Donal D C Bradley,* Wei Huang**

[#]Q. Zhang and J. Liu contributed equally to this work.

Q. Zhang, J. Liu, Q. Wie, X. Guo, Y. Xu, Prof. R. Xia, Prof. L. Xie, Prof. Y. Qian
Key Laboratory for Organic Electronics and Information Displays (KLOEID)
Institute of Advanced Materials (IAM)
Jiangsu National Synergetic Innovation Center for Advanced Materials (SICAM)
Nanjing University of Posts & Telecommunications
9 Wenyuan Road, Nanjing 210023, China
E-mail: iamrdxia@njupt.edu.cn, iamyqian@njupt.edu.cn

C. Sun, Dr L. Lüer, Dr. J. Cabanillas-Gonzalez
Madrid Institute for Advanced Studies (IMDEA Nanociencia)
Calle Faraday 9, Ciudad Universitaria de Cantoblanco, Spain
E-mail: juan.cabanillas@imdea.org

Prof. D. D. C. Bradley
Departments of Engineering Science and Physics,
Division of Mathematical, Physical and Life Sciences,
University of Oxford, 9 Parks Road, Oxford OX1 3PD, UK
E-mail: Donal.Bradley@mpls.ox.ac.uk

Prof. W Huang
Shanxi Institute of Flexible Electronics (SIFE), Northwestern Polytechnical University (NPU),
127 West Youyi Road, Xian, 710072, P.R. China
E-mail: iamwhuang@nwpu.edu.cn

Keywords: conjugated polymer, Förster resonant-energy-transfer, stimulated emission, exciton confinement, photoinduced absorption

Abstract: We report state-of-the-art fluorene-based yellow-green conjugated polymer blend gain media using Förster resonant-energy-transfer (FRET) from novel blue-emitting hosts to yield low threshold ($\leq$ 7 kW cm^{-2}) lasers operating between 540 and 590 nm. For poly(9,9-dioctylfluorene-*co*-benzothiadiazole) (F8BT) (15 wt.%) blended with our newly synthesised 3,6-*bis*(2,7-di([1,1'-biphenyl]-4-yl)-9-phenyl-9H-fluoren-9-yl)-9-octyl-9H–carbazole (DBPhFCz) a highly desirable more than four-times increase (relative to F8BT) in net optical gain to 90 cm^{-1} and thirty four-times reduction in amplified spontaneous emission threshold to 3 μJ cm^{-2} is achieved. Detailed transient absorption studies confirm effective exciton

confinement with consequent diffusion-limited polaron-pair generation for DBPhFCz. This delays formation of host photoinduced absorption long enough to enable build-up of the spectrally overlapped, guest optical gain and resolves a longstanding issue for conjugated polymer photonics. Our comprehensive study further establishes that limiting host conjugation length is a key factor therein, with 9,9-dialkylfluorene trimers also suitable hosts for F8BT but not pentamers, heptamers or polymers. We additionally demonstrate that the host highest occupied and lowest unoccupied molecular orbitals can be tuned independently from the guest gain properties. This provides the tantalizing prospect of enhanced electron and hole injection and transport without endangering efficient optical gain; a scenario of great interest for electrically pumped amplifiers and lasers.

1. Introduction

Conjugated polymers with high photoluminescence quantum efficiencies (PLQEs) and spectrally broad stimulated emission (SE) cross-sections are attractive gain media for solid-state lasers and optical amplifiers.[1-6] These and other organic gain media can be pumped by compact laser- (LD)[7-10] and light-emitting- (LED)[11, 12] diode sources but direct electrical pumping has not been reported yet. Binary blends of conjugated host and guest materials have been used both to enhance LED performance and to reduce optically pumped laser thresholds via efficient exciton generation on the host and/or guest and rapid host-to-guest FRET. In the case of LEDs, and future LDs, effective charge injection and transport are also key. Many such blend systems have been reported, including polymer:polymer[13-17] and dye:polymer[8] blends but no fluorene-based-lasing systems that operate in the yellow-green.

The poly(9,9-dioctylfluorene) (PFO) blue-emission host: poly(9,9-dioctylfluorene-*co*-benzothiadiazole) (F8BT) yellow-green-emission guest blend system has been extensively used for efficient LEDs, with FRET-based PLQE values ≤ 70%.[18-21] However, the same

PFO:F8BT blend system does not yield efficient optical gain. ASE can be observed for certain compositions and pumping regimes but only with very high thresholds. For example E_{th}^{ASE} = 200 – 390 μJ cm^{-2} for 5, 10, 90 and 95 wt.% F8BT blends pumped at 337 nm with 3ns, 10Hz, N_2 laser pulses but there is no ASE for 25, 50 and 75 wt.% blends even when pumped at up to 15 mJ cm^{-2}.[22] This is despite efficient FRET being evident for all PL spectra (Supporting Information (SI) **Figure S1**). A similar situation arises for other blue (fluorene-based) hosts, including arylamine-containing hole-injection copolymers.[23]

At first sight it seems anomalous that such high exciton-derived PLQE should not yield efficient optical gain. However, pump-probe transient spectroscopy studies on PFO reveal photoinduced absorption (PA) within the 540 to 590 nm PL range of F8BT.[24-27] This band, designated PA_p, is assigned to weakly-coupled polaron-pair charge states that rapidly form (< 150 fs)[24] at the expense of excitons; the spectral match to electrochemical-oxidation-induced steady-state differential absorbance (ΔA) confirms the charge.[28] This PA_p is intense (100 nm films give $\Delta A \approx 10^{-3}$ (i.e. $\Delta\alpha \approx 10^2$ cm^{-1}) at 500 fs) and its duration is largely governed by on-chain picosecond recombination.[29] A diminished PA_p signature can persist beyond 100 ps but only as a consequence of infrequent inter-chain charge transfer and/or polaron trapping processes.[30] Consequently, the F8BT SE resulting from FRET faces overwhelming competition (on the short timescales that matter) from host PA, curtailing the prospects for lasing.

This situation has been known for more than a decade but no solutions have emerged despite enduring interest in F8BT for LEDs, light-emitting transistors (LETs) and as a potential LD gain-medium.[31-34] We now report a novel host, namely 3,6-*bis*(2,7-di([1,1'-biphenyl]-4-yl)-9-phenyl-9H-fluoren-9-yl)-9-octyl-9H–carbazole (DBPhFCz), a thermally stable (T_g > 240 °C) H-shaped molecule, consisting of *bis*-aryl-substituted-fluorene arms bridged at the C9-

position by a carbazole unit. DBPhFCz possesses state-of-the-art blue lasing properties[4,34] and, more importantly, has a substantially weaker PA_p than PFO, with a grow-in time that further limits competition, thereby yielding efficient FRET-pumped F8BT SE and lasing. We additionally demonstrate, through a detailed study of different length 9,9-dihexylfluorene oligomers and an aryl-substituted terfluorene, that this is a general behavior in short conjugation length hosts, confirming that exciton confinement helps to prevent rapid-onset PA_p and thus facilitates guest SE. Our results resolve a longstanding puzzle in conjugated polymer photonics and offer an avenue to progress with electrical pumping,[32] strengthened by the finding that the confined-exciton-host approach allows a decoupling of host highest occupied/lowest unoccupied molecular orbital (HOMO/LUMO) energies from guest optical gain. They also bring the yellow-green spectral window into line with the blue and red ranges in terms of available fluorene-based gain media. Finally, these results place a question mark over the explanation given for oxygen-quenching-related gain-enhancement in oligofluorene-based liquid lasers.[35, 36]

2. Results and Discussion

2.1 Pump-probe transient spectroscopy of host materials and blends

The chemical structures of F8BT, PFO and DBPhFCz are presented in **Figure 1** together with absorption, PL and amplified spontaneous emission (ASE) spectra. The PL spectra of PFO and DBPhFCz strongly overlap with the longer wavelength (461 nm peak) F8BT absorption band, promoting efficient FRET to F8BT as confirmed by the F8BT-dominated PL spectra of blends (SI Figure S1).

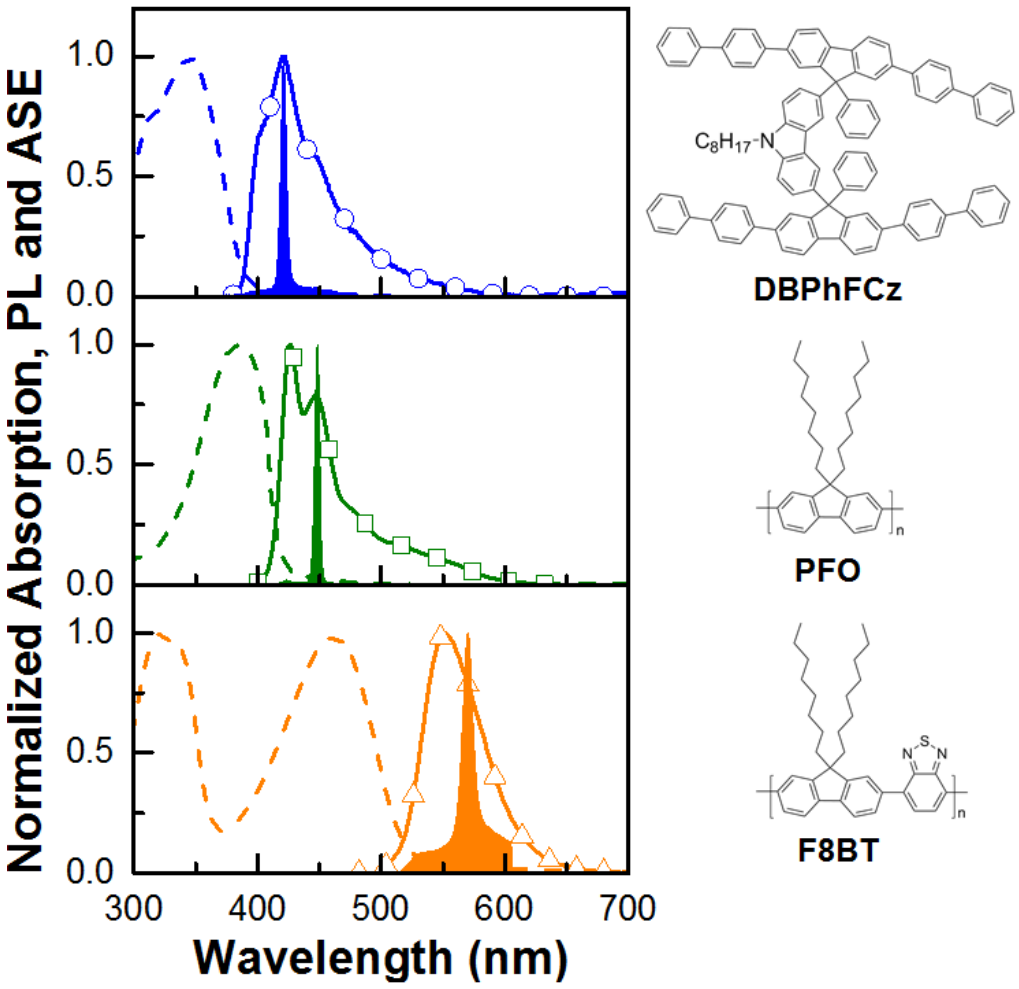

Figure 1: Peak normalized thin film absorption (dashed line), photoluminescence (solid line and symbols) and ASE (in-filled) spectra for DBPhFCz (upper panel), PFO (middle panel) and F8BT (lower panel). Corresponding chemical structures are shown on the right. DBPhFCz absorption peaks at 350 nm, vibronically-structured PL at 420 (S_1 to S_0 (0-1)) with shoulders at 402 ((0-0)) and 445 ((0-2)) nm and ASE at 420 nm. PFO absorption peaks at 390 nm, PL at 425 (S_1 to S_0 (0-0)) and 450 ((0-1)) nm, with ASE at 450 nm. F8BT absorption peaks at 330 and 461 nm, PL at 551 nm and ASE at 570 nm (close to a poorly resolved PL shoulder).

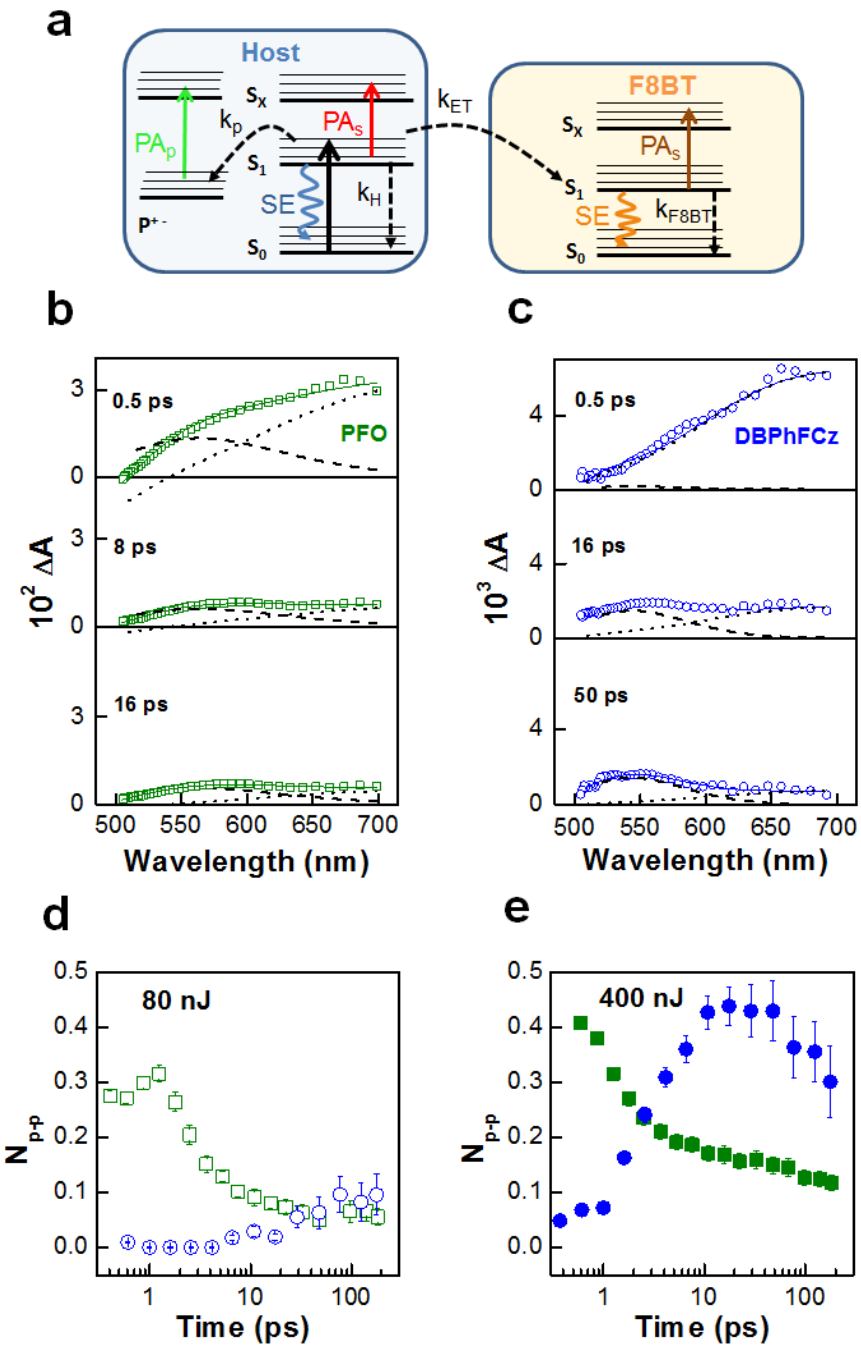

Figure 2: Transient absorption spectra for PFO and DBPhFCz. (a) Energy level schematic for blue-emitting host (left) and F8BT guest (right). Representative (b) PFO (green open squares) and (c) DBPhFCz (blue open circles) thin film pump-probe spectra (excited with 120 fs, 80 nJ (66 μJ cm^{-2}) pulses at 387 nm) are plotted as differential absorbance (ΔA) data. Spectra are shown in both cases for three pump-probe time delays selected to illustrate the ΔA temporal evolution. Note different ordinate scales. Discontinuous black lines show fitted spectral weights (see SI) for singlet exciton (dotted) and polaron-pair (dashed) contributions and thin green/blue solid lines through the data show resulting combined fits. Time-dependent polaron-pair concentrations per absorbed photon ($N_{p\text{-}p}$) are also shown for PFO (green squares) and DBPhFCz (blue circles), under (d) 80 nJ (open symbols) and (e) 400 nJ (filled symbols) pulse excitation. $N_{p\text{-}p}$ values were deduced (see SI) from corresponding ΔA data.

Figure 2(a) shows a schematic energy level diagram for preferential host (left panel) photoexcitation. Singlet exciton and polaron levels are labelled S_X and P^{+-}, respectively. Pump-probe optical transitions are depicted as vertical solid up-arrows, excited-ground state decay as vertical dashed down-arrows, SE as wavy solid down-arrows and other (charge/energy) transfer processes as arched down-arrows. S_0-S_1 pump absorption is shown as a black up-arrow. Charge dissociation leading to polaron-pair PA_p (green up-arrow, P^{+-} manifold) occurs from S_1 with rate k_p (dashed black arched down-arrow) and host S_1-S_0 decay (dashed black down-arrow), with rate k_H. Exciton S_1-S_X PA_s (red up-arrow) and SE (blue wavy down-arrow) also contribute to the host spectra. Conversely, host triplet states are not evident in the spectral data and are not, therefore, represented in the schematic. Host-to-guest FRET to F8BT (dashed black arched down-arrow to right panel) occurs with rate k_{ET}, resulting in guest PA_s (brown up-arrow), SE (yellow wavy down-arrow) and S_1-S_0 decay (dashed black down-arrow, rate k_{F8BT}). Figures 2(b) and (c) show, respectively, PFO and DBPhFCz 500-700 nm pump-probe transient spectra. More comprehensive data sets and corresponding F8BT data are in SI **Figure S2.** ΔA in this range should contain spectral signatures of singlet excitons (SE and PA_s) and polaron-pairs (PA_p) and the data was modelled (see SI **Figure S3**) at each time-delay as a simple combination thereof. There was no need to include other contributions. In particular no triplet PA (PA_T) was evident; DBPhFCz PA_T is manifested in quasi-steady-state as a sharp ~ 655 nm peak which closely resembles PA_T for terfluorenes[35] whilst in PFO it is likewise sharp but at ~ 860 nm (SI **Figure S4**). An absence of DBPhFCz PA_T for delays up to 400 ps (data not shown) is consistent with inter-system crossing only on longer timescales.

Focusing first on Figure 2(b), the 0.5 ps PFO ΔA spectrum can be fit with strong PA_p ($\Delta A(565\text{ nm}) = 1.3 \times 10^{-2}$), even stronger PA_s ($\Delta A(690\text{ nm}) = 2.8 \times 10^{-2}$) and SE below ~540 nm ($\Delta A(518\text{ nm}) = -0.65 \times 10^{-2}$); in agreement with previous reports.[24, 26] Clearly, at 0.5 ps

singlet excitons and polaron-pairs coexist, confirming impulsive-like polaron photogeneration.[24, 29, 30, 37] At 8 and 16 ps delays the overall ΔA magnitude decreases but can still be fitted to PA_p, PA_s and SE components. At 16 ps PA_p ΔA(565 nm) = 0.58 x 10^{-2}, PA_s ΔA(690 nm) = 0.46 X 10^{-2} and SE ΔA(518 nm) = -0.12 x 10^{-2}. The spectrum thus evolves to be increasingly characteristic of PA_p, consistent with faster singlet than polaron-pair decay (see also SI **Figure S5**).

Conversely, the DBPhFCz ΔA spectrum (Figure 2(c)) is dominated at 0.5 ps by PA_s, with PA_p only appearing at longer delays (16 and 50 ps). Note also that as DBPhFCz SE occurs at 390 - 455 nm it does not contribute to these spectra. At 0.5 ps, PA_s gives ΔA (690 nm) = 6.3 x 10^{-3} whereas PA_p gives only ΔA (543 nm) = 0.05 x 10^{-3}. At 50 ps delay PA_s falls to ΔA(690 nm) = 1.4 x 10^{-3}, with PA_p then contributing ΔA (543 nm) = 0.8 x 10^{-3}. DBPhFCz polaron-pair formation is not therefore an impulsive process; the population instead grows-in over many ps (see also SI Figure S5).

A more quantitative picture is provided by the polaron-pair concentration per absorbed photon, $N_{p\text{-}p}$ (see SI for details). Figures 2(d) and (e) display the extracted $N_{p\text{-}p}(t)$ values from t = 400 fs to 200 ps for PFO and DBPhFCz. Since phenylene-polymer polaron-pair generation is intensity dependent,[37] we compared measurements at both low ((d); 80 nJ $pulse^{-1}$/66 μJ cm^{-2}) and high ((e); 400 nJ $pulse^{-1}$/330 μJ cm^{-2}) pulse energy/energy density. For PFO at 80 nJ pulse energy, $N_{p\text{-}p}$ increases from ≈ 0.28 at 400 fs to ≈ 0.32 at 1.6 ps before decaying with both fast (2.3 ± 0.2 ps) and slow (504 ± 256 ps) time constants. At 400 nJ, $N_{p\text{-}p}$(600 fs) ≈ 0.4, with no initial rise and slightly faster 1.4 ± 0.1 ps and 374 ± 47 ps decays. In contrast, for DBPhFCz at 80 nJ, $N_{p\text{-}p}$(400 fs) is below the detection sensitivity and even at 400 nJ $N_{p\text{-}p}$(600 fs) only reaches ≈ 0.07. The $N_{p\text{-}p}$ build-up time at 80 nJ is 22 ± 8 ps, revealing the likely role of exciton diffusion in polaron photogeneration.[38] Interestingly, with 400 nJ pulses, the polaron-

pair population builds up more quickly (4 ± 2 ps) but then peaks at 18 ps as recombination onsets.

The all-important negligible/low initial $N_{p\text{-}p}$ turns out to be a general feature of short conjugation length hosts; the same behavior occurs for 9,9-dihexylfluorene trimer (3F6) (SI **Figures S7 and S8**) and for another novel oligomer 9,9,9'',9''-tetraoctyl-9'-phenyl-9'-(3-(N-octyl-carbazole))-2,2':7',2''-terfluorene (TrFCz) (SI **Figures S9 and S10**), a molecule intermediate between 3F6 and DBPhFCz. Just as for DBPhFCz, the initial (0.4 ps) ΔA (SI Figure S10) is dominated by singlet exciton contributions with weak PA_p that builds-up slowly, over tens of ps. The 3F6 polaron-pair concentration is even lower; negligible for 80 nJ excitation and only reaching $N_{p\text{-}p} \leq 0.08$ for 400 nJ per pulse (SI Figure S8).

We attribute the differences between PFO and DBPhFCz to relative exciton confinement, consistent with previous observations that polymer polaron-pair formation can be prevented by chain isolation.[27, 29, 38, 39] The short DBPhFCz conjugation length together with its bulky, non-planar shape introduces a large degree of confinement, countering geminate-pair separation and reducing substantially charge generation rate (k_p). Polaron-pairs will still form via diffusion-controlled processes that lead to dissociation at randomly encountered sites with suitable (structure-derived) offsets in HOMO/LUMO energy[40] and/or via exciton-exciton annihilation[41] but on significantly longer timescales. Such sites are also expected to be less numerous for the more glass-like DBPhFCz host.

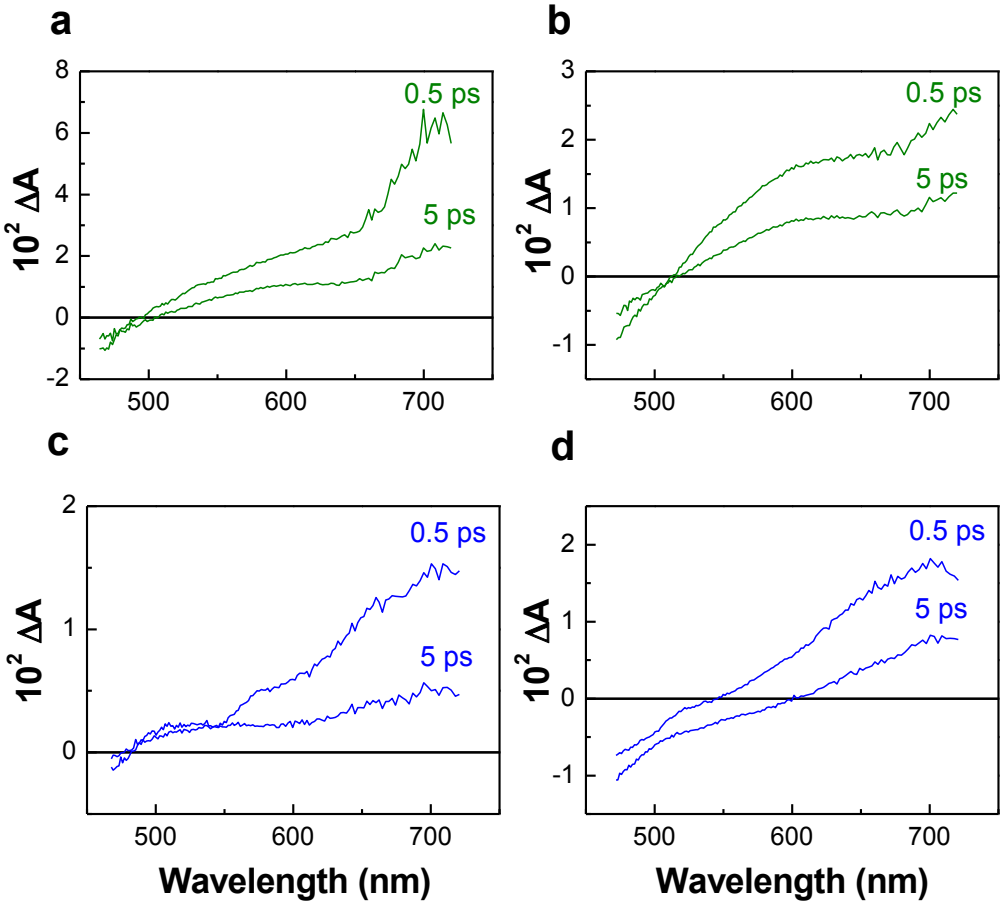

Figure 3: Pump-probe spectra for F8BT blends with PFO (upper panels) and DBPhFCz (lower panels). Data are shown for (a) 1 wt.% and (b) 20 wt.% F8BT with PFO and (c) 1 wt.% and (d) 20 wt.% F8BT with DBPhFCz at 0.5 ps and 5 ps pump-probe delays following excitation at 387 nm with 150 fs, 200 nJ pulse^{-1} (165 μJ cm^{-2}). Note different ordinate scales. Weak spectral evolution is inferred when comparing ΔA at 0.5 and 5 ps (there are no new contributions over time) and the positive ΔA observed in the F8BT PL range $\lambda \approx 500 - 610$ nm) confirms that PFO-based PA_p overwhelms FRET-pumped F8BT SE. The amplitude evolution further shows that this PA_p is strongest at shorter times. In the 1 wt.% F8BT with DBPhFCz blend the ΔA spectra at 0.5 and 5 ps both show the spectral features of DBPhFCz singlet excitons and polaron-pairs as well as a contribution from F8BT singlet PA_s. This implies a modest FRET rate from DBPhFCz to F8BT at low guest concentration. In the 20 wt.% F8BT with DBPhFCz blend, however, the 5 ps delay spectrum shows that F8BT SE can in that case overcome DBPhFCz PA_p.

Further confirmation of the host-exciton-confinement effect is obtained by comparison of ΔA spectra (SI Figure S8) for 3F6 with 5F6 and 7F6 (respectively 5- and 7-unit 9,9-dihexylfluorene oligomers). For 5F6 and 7F6, unlike 3F6, 'impulsive' polaron-pair photogeneration is observed, with higher quantum yield for the longer oligomer. Exciton confinement in long-chain polymer hosts might then require intra-chain segmentation (e.g. insertion of *m*-phenylene rings)[42] with a high proportion of conjugation-breaks.

Importantly, the delayed polaron-pair build-up in DBPhFCz allows, even at high excitation density, a sufficient temporal window that FRET can support F8BT SE. This is evidenced in the PFO:F8BT and DBPhFCz:F8BT blend ΔA spectra (**Figure 3**) for 1 wt.% and 20 wt.% F8BT. In both PFO:F8BT blends ΔA is characterized by F8BT ground state photobleach (PB) in the 480 – 518 nm spectral range and PA in the 520 – 730 nm spectral region comprising overlapping PFO PA_p (520 – 699 nm) and F8BT PA_s (590 – 730 nm). SI Figure S2 shows the corresponding undiluted (100 wt.%) F8BT PB, SE and PA_s spectra. The resolutely positive ΔA(565 nm) PA_p-dominated-signal observed in Figure 3(a-c) is consistent with an absence of ASE in those blends (discussed further below; see **Figure 5**). In contrast, the 5 ps ΔA spectrum for 20 wt.% F8BT in DBPhFCz shows negative ΔA (518 – 605 nm), from yellow-green F8BT SE, followed by F8BT PA_s (605 – 720 nm). These data nicely illustrate how the balance (c.f. Figure 2(a)) between k_p and FRET (k_{ET}) determines blend optical gain; the 1 wt.% DBPhFCz:F8BT blend has insufficient F8BT to support efficient FRET (consistent with the steady state spectral data for blend PL in SI Figure S1). Further consistent with these data, we find that 3F6:F8BT and TrFCz:F8BT blends both exhibit F8BT SE (c.f. SI Figures S8 and S10), whilst blends with longer oligomer hosts (5F6:F8BT and 7F6:F8BT) show dominant PA_p instead (c.f. SI Figure S8).

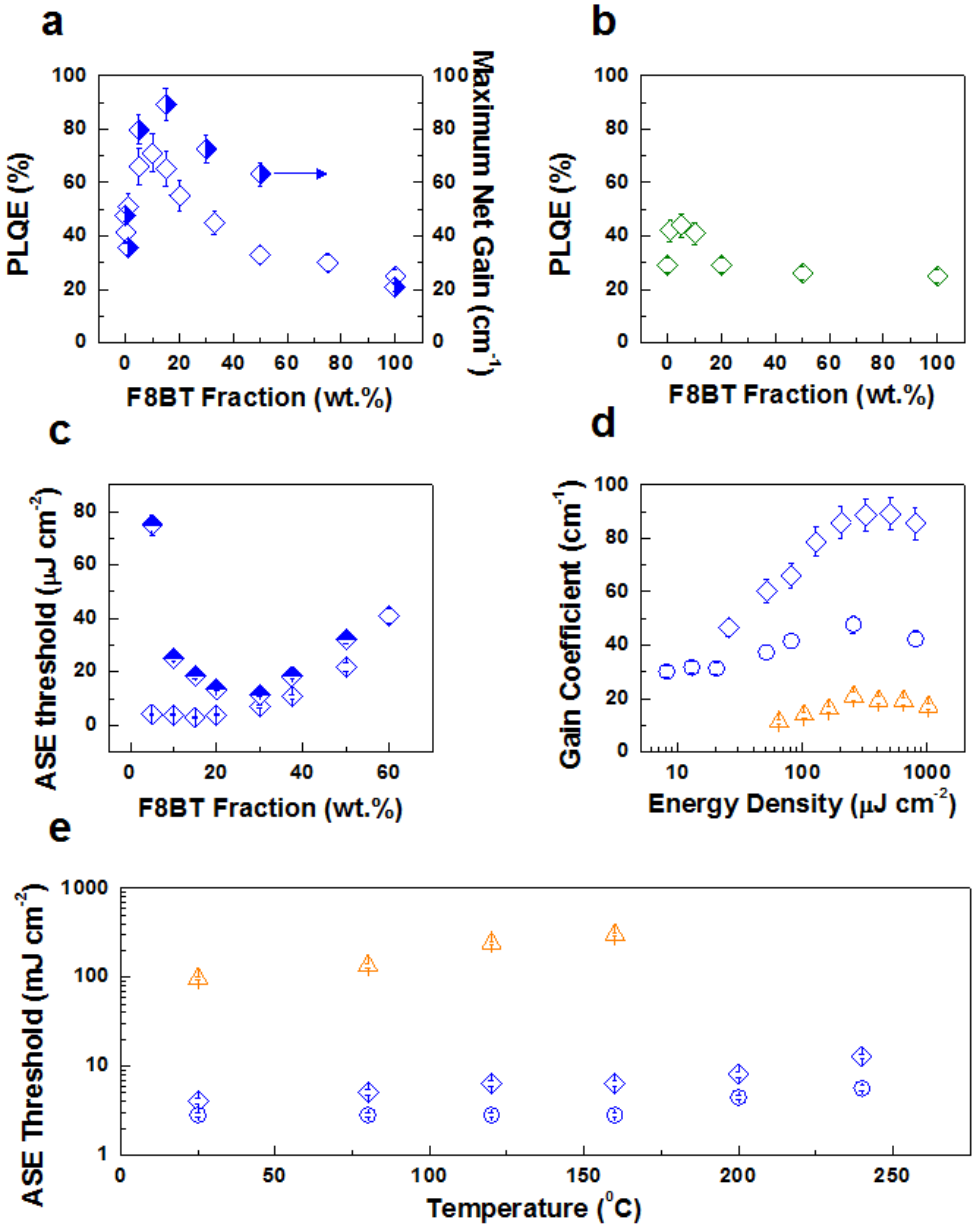

Figure 4: PLQE and optical gain characteristics for F8BT blends with PFO and DBPhFCz. (a) DBPhFCz:F8BT blend PLQE (blue open diamonds, left ordinate, λ_{exc} = 370 nm) and g_{max} (half-filled right-diamonds, right ordinate, λ_{exc} = 370 nm for host and blends, λ_{exc} = 450 nm for F8BT) plotted as a function of F8BT fraction. (b) PFO:F8BT blend PLQE (green open diamonds, λ_{exc} = 370 nm). (c) DBPhFCz:F8BT blend E_{th}^{ASE} for both FRET-dependent host (λ_{exc} = 370 nm, open diamonds) and direct guest (λ_{exc} = 450 nm, half filled up-diamonds) pumping, plotted *vs* F8BT fraction up to 60 wt.%. (d) Net gain coefficients, *g*, for DBPhFCz:F8BT (15 wt.%) blend (blue open diamonds), 100% DBPhFCz (blue open circles) and 100% F8BT (orange open up-triangles), plotted *vs* pump energy density (log scale); λ_{exc} = 370 nm for blend and DBPhFCz and λ_{exc} = 450nm for F8BT. (e) Influence of thermal annealing on E_{th}^{ASE} values (log scale) for DBPhFCz (open circles), F8BT (open up-triangles) and a DBPhFCz:F8BT (10 wt.%) blend (open diamonds).

2.2 PL and optical gain properties of host materials and blends

The absorption and PL spectra of DBPhFCz:F8BT and PFO:F8BT films with 0, 1, 5, 10, 20, 50 and 100 wt.% F8BT are shown in SI Figure S1 together with atomic force microscopy (AFM) images. Effective FRET occurs for both series with emission quickly dominated by F8BT.

Figure 4(a) shows DBPhFCz:F8BT film PLQEs plotted *vs* F8BT fraction. 100 wt.% DBPhFCz and F8BT give PLQE ≈ 40% and 25%, respectively. As F8BT fraction increases, PLQE also initially increases, from 41% at 0 to 51% at 1 and 70% at 10 wt.%, then falls for higher fractions, to 32% for 50 wt.% and then more slowly to 25% for F8BT. This tendency is also found in the PFO:F8BT films (Figure 4(b), peak PLQE = 44% for 5 wt.% F8BT) and is typically reported for other FRET-coupled host:guest systems, signaling a trade-off between the efficiency of FRET and guest self-quenching.[43,44] However, no ASE was detected in PFO:F8BT blends when pumped at 370 nm with pulse energies up to 50 μJ (2330 μJ cm^{-2}) irrespective of F8BT fraction.

Figure 4(c) shows the corresponding DBPhFCz:F8BT ASE threshold (E_{th}^{ASE}) dependence. The 100 wt.% F8BT had $E_{th}^{ASE} \approx 2.7$ μJ $pulse^{-1}$ (96 μJ cm^{-2}) for $\lambda_{exc} = 450$ nm pumping but no spectral narrowing was observed up to 3 μJ $pulse^{-1}$ for $\lambda_{exc} = 370$ nm. For selective guest ($\lambda_{exc} = 450$ nm) photoexcitation E_{th}^{ASE} initially decreases with F8BT fraction from 5 wt.% ($E_{th}^{ASE} = 75$ μJ cm^{-2}) to 30 wt.% and then increases again, consistent with a trade-off between insufficient guest absorption/gain at low fractions and subsequent concentration quenching.[13,45,46] The lowest $E_{th}^{ASE} = 319$ nJ $pulse^{-1}$ (11.4 μJ cm^{-2}) is less than one eighth $E_{th}^{ASE} = 2.7$ μJ $pulse^{-1}$ (96 μJ cm^{-2}) for 100 wt.% F8BT ($\lambda_{exc} = 450$ nm). E_{th}^{ASE} is further reduced by host-excitation ($\lambda_{exc} = 370$ nm) and FRET to F8BT; for 15 wt.% F8BT, E_{th}^{ASE} =

60 nJ pulse^{-1} (2.8 μJ cm^{-2}), 34-fold lower than 100 wt.% F8BT (λ_{exc} = 450 nm). In addition, for λ_{exc} = 370 nm there is no strong increase in E_{th}^{ASE} below the 15 wt.% 'sweet-spot'; the absorbed photon flux is host- not guest-dominated. Eventually, at ≤ 1 wt.% F8BT, FRET no longer dominates over DBPhFCz emission (see SI Figure S1) and 418 nm host ASE emerges. Conversely, guest self-quenching increases E_{th}^{ASE} for ≥ 30 wt.% F8BT. Typical DBPhFCz:F8BT (5 - 50 wt.% F8BT) and F8BT ASE spectra are shown in SI Figure S6 and **Table 1** summarizes key parameters for selected samples.

Table 1: Key laser gain parameters for DBPhFCz, F8BT and DBPhFCz:F8BT blends with 1, 5 and 15 wt.% F8BT. α is the absorption coefficient; *PLQE* is the PL quantum efficiency (λ_{exc} = 370 nm) for emission in the given range; τ is the PL decay time; $\boldsymbol{\lambda_{ASE}}$ is the ASE peak position; E_{th}^{ASE} is the threshold pump energy (at which FWHM linewidth of emission spectrum halves); g_{max} is the maximum gain coefficient, E_{th}^{laser} is the laser threshold; $\Lambda_{grating}$ is the DFB grating period; and λ_{laser} is the resulting laser tuning range.

	DBPhFCz	**1%**	**5%**	**15%**	**F8BT**
$\boldsymbol{\alpha}$ (10^5 cm^{-1}) @ (a) 370 nm (b) 450 nm	(a) 1.26	(a) 1.23 (b) 0.017	(a) 1.21 (b) 0.07	(a) 1.08 (b) 0.18	(a) 0.27 (b) 1.47
PLQE (%) & range (nm)	41% 390 – 500	51% 500 – 630	66% 500 – 630	65% 500 – 630	25% 500 – 630
$\boldsymbol{\tau}$ (ns)	-	-	2.74	1.94	0.72
λ_{ASE} (nm)	418	417	557	561	570
E_{th}^{ASE} (μJ cm^{-2}) pumped @ (a) 370 nm (b) 450 nm	(a) 2.1	(a) 9.2	(a) 4.2 (b) 75	(a) 2.8 (b) 19	(b) 96
g_{max} (cm^{-1})	48	36	80	90	20
E_{th}^{laser} @ λ (nm) (a) nJ pulse^{-1} (b) μJ cm^{-2} (c) kW cm^{-2}	(a) 2.5 (b) 9.7 (c) 2.0 @ 416 nm	-	(a) 4.9 (b) 19.3 (c) 6.4 @ 552 nm	(a) 2.5 (b) 9.8 (c) 3.3 @ 561 nm	(a) 35 (b) 138 (b) 43 @ 564 nm
$\Lambda_{grating}$ (nm)	250	-	350	350	350
λ_{laser} (nm)	402 - 440	-	539 - 552	545 - 579	551 - 581

The maximum DBPhFCz:F8BT gain coefficients, g_{max}, plotted *vs* F8BT fraction in Figure 4(a) show a similar form to the corresponding PLQE data albeit with the peak at slightly higher F8BT fraction and a more linear subsequent fall to the F8BT value; 15 wt.% F8BT gives the maximum c.f. 10 wt.% for PLQE. Figure 4(d) shows the associated *g(E)* dependence for host DBPhFCz, guest F8BT and optimal 15 wt.% F8BT blend. The blend $g_{max} \approx 90$ cm^{-1}, obtained at ~ 7 μJ pulse^{-1}, represents ≈ 4.5-fold increase over F8BT (20 cm^{-1}).[45] $\lambda_{exc} = 370$ nm was employed for DBPhFCz and blends and $\lambda_{exc} = 450$ nm for F8BT. g_{max} values for DBPhFCz, F8BT and selected blends are collected in Table 1.

Host-to-guest FRET can, therefore, indeed be effective to enhance yellow-green F8BT optical gain but only with appropriate hosts that avoid competing PA_p. PFO:F8BT blends do not show ASE even when pumped at 5 μJ pulse^{-1} (227 μJ cm^{-2}, >> E_{th}^{ASE} host/guest alone), consistent with ΔA and previous studies. This confirms that whilst FRET is necessary and significant steady-state PLQE indicative, they are not sufficient for guest SE. TrFCz:F8BT works well (SI Figure S9), as also does 3F6:F8BT (SI Figure S7), although in the latter case crystallization and phase separation rapidly degrade performance. Conversely, no optical gain was obtained for 5F6:F8BT and 7F6:F8BT, in agreement with a lack of F8BT SE in ΔA spectra (SI Figure S8).

Importantly, the outstanding F8BT-based optical gain properties of blends with both DBPhFCz and TrFCz (Figures 4 and SI Figures S10), despite their substantially different HOMO/LUMO levels (-5.67/-2.35 eV and -5.09/-1.95 eV respectively), signals the opportunity to significantly engineer charge injection for our confined exciton host blends without negative impact on guest optical gain.

Under continuous optical pumping (at ~ 8 x E_{th}), the 15 wt.% DBPhFCz:F8BT blend exhibits rather stable ASE behaviour for more than 4 hours (SI Figure S6(f)) before notable degradation onsets. DBPhFCz and 10 wt.% DBPhFCz:F8BT also show admirable thermo-oxidative stability with only moderate increases in E_{th}^{ASE} upon annealing to 240 °C in air (see Figure 4(e)), consistent with $T_g \approx 308$ °C (SI **Figure S11**). Film microstructure was scarcely affected at 200 °C (SI Figure S1) whereas for F8BT ($T_g \approx 120$ °C) surface roughening accompanies a 3-fold E_{th}^{ASE} increase at 150 °C (SI Figure S1).

To further emphasize the importance of the host we compare in Figure 5(a) and (b), respectively, the 387 nm, 120 fs, 400 nJ pulse-pumped, 565 nm ΔA temporal evolution for DBPhFCz:F8BT and PFO:F8BT with 1, 5, 10, 20 and 50 wt.% F8BT. These data show that for DBPhFCz:F8BT with ≥ 10 wt.% F8BT, guest SE builds up in < 2 ps. For 1 wt.% F8BT slow DBPhFCz-to-F8BT FRET leads instead, as also for all PFO:F8BT blends, to dominant host PA_p.

Fitting 400 nJ pump DBPhFCz:F8BT blend SE (see SI for details) yields k_{ET} = 0.2 - 4.5 ps^{-1} (Figure 5(c)), with FRET times accordingly shorter than the 4 ps DBPhFCz PA_p build-up for all but the 1 wt.% blend. Subsequent F8BT singlet decay rates (k_{F8BT}) (Figure 5(d)) are ≈ 10^{-2} ps^{-1} and less concentration-dependent. The difference from reported PL decay times (1.5 - 2 ns)[24, 45] arises from a 100-fold higher excitation density with consequent SE and exciton-exciton annihilation.[27] Comparison of ΔA dynamics for 200 and 400 nJ $pulse^{-1}$ excitation supports this; k_{ET} changes little (Figure 5(c)) suggesting exciton-exciton annihilation does not compete significantly with FRET but k_{F8BT} increases approximately four-fold (Figure 5(d)) consistent with a significant role in F8BT exciton-decay.

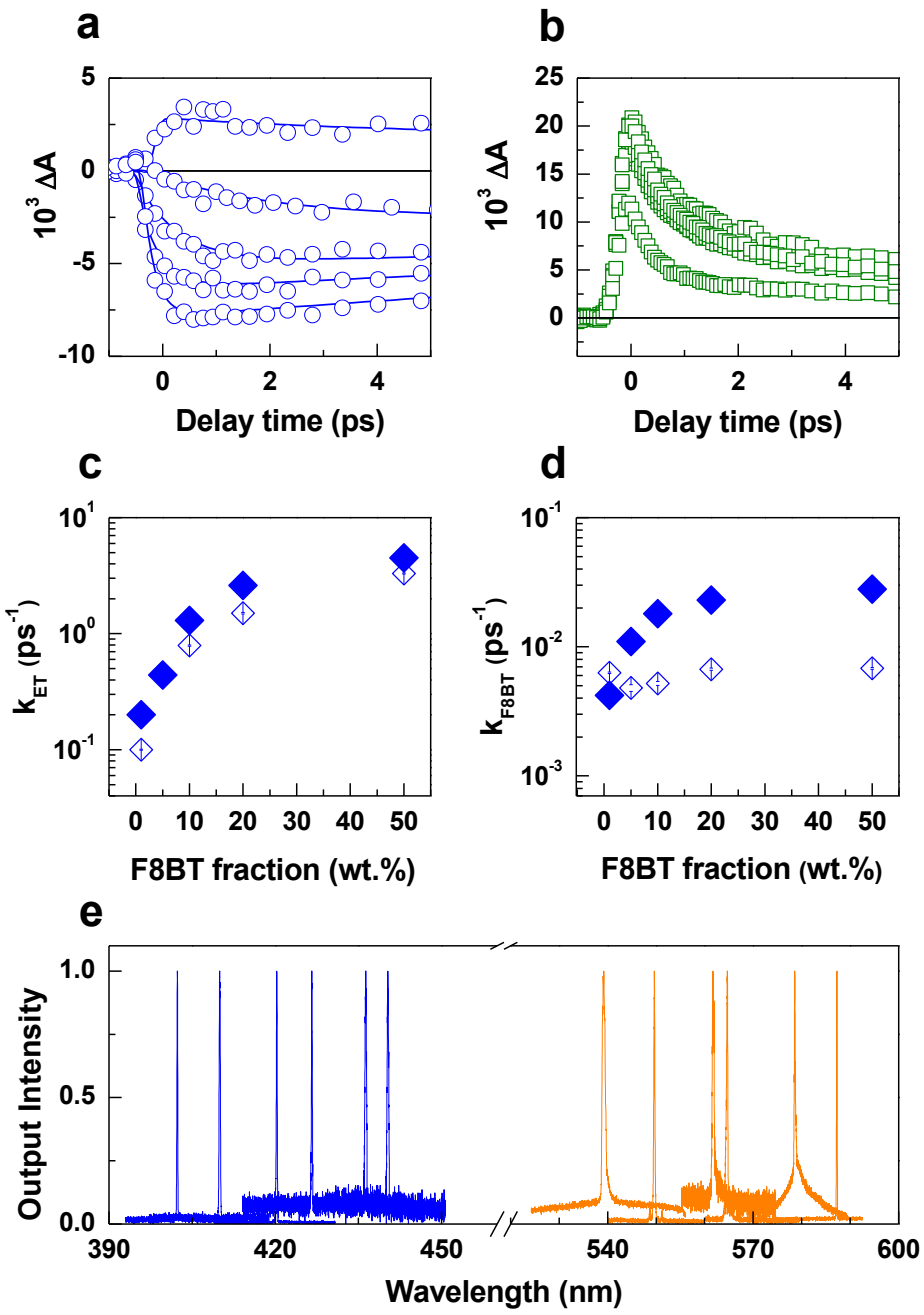

Figure 5: Excited state dynamics, FRET energy transfer and guest singlet S_1-decay rates, and DFB laser spectra for F8BT blend films. Temporal evolution of (a) DBPhFCz:F8BT (open circles) and (b) PFO:F8BT (open squares) blend ΔA(565 nm) transient absorption parametric in F8BT fraction; dynamics correspond to (from top to bottom) 1, 5, 10, 20 and 50 wt.%. Excitation was at 387 nm with 200 nJ (165 μJ cm^{-2}) per pulse. Also shown are fits (solid lines) to the excited state dynamics model described in SI. Note different ordinate scale. (c) k_{ET} and (d) k_{F8BT} values (log scale) deduced from the fits to the ΔA data for DBPhFCz:F8BT blends. Note different ordinate scales. The rates are shown for two pump pulse energies: 200 nJ (open diamonds) and 400 nJ (filled diamonds). (e) 2nd order DFB laser spectra for DBPhFCz:F8BT blends (539 to 587nm, orange lines). Data are also shown for undiluted (100 wt.%) DBPhFCz (402 to 440nm, blue lines). Wavelength tuning was achieved in the former case by F8BT fraction (5, 15 and 60 wt.%) and film thickness (130 to 235 nm) and in the latter by thickness alone (53 to 163 nm).

2.3 DBPhFCz and F8BT blend Laser emission

As a final step, we fabricated optically-pumped, surface-emitting distributed feedback (DFB) lasers by spin-coating DBPhFCz and DBPhFCz:F8BT blend films on top of one-dimensional (1-D), etched-fused-silica gratings. Figure 5(e) shows laser spectra systematically tuned via spin-coated film thickness and blend composition. The 1 - 2 nm full-width-half-maximum linewidth is instrument limited. For DBPhFCz, the laser peak can be thickness-tuned from ~ 400 to 440 nm, with lowest threshold (SI Figure S6), $E_{th}^{laser} \approx 2$ nJ pulse^{-1} (i.e. 9.7 μJ cm^{-2} / 2.03 kW cm^{-2}), achieved for 416 nm lasing (85 nm film thickness). For DBPhFCz:F8BT, as anticipated, yellow-green lasing is achieved across ~ 540 - 590 nm using 5, 15 and 60 wt.% blends and film thicknesses 130 nm (5 wt.%), 130 nm, 150 nm, 175 nm, 190 nm (15 wt.%) and 235 nm (60 wt.%). The lowest $E_{th}^{laser} \approx 2.49$ nJ pulse^{-1} (i.e. 9.79 μJ cm^{-2}/ 3.26 kW cm^{-2}) occurs for 561 nm lasing, using 15 wt.%, 175 nm thickness films. In addition, in line with ΔA and ASE measurements, TrFCz:F8BT and 3F6:F8BT blend DFB structures also exhibit lasing (data not shown).

3. Conclusion

This paper has addressed the long-standing question why polyfluorene host:F8BT guest blend systems with high-PLQE yellow-green PL and excellent LED characteristics nevertheless show disappointingly poor optical gain and no lasing. Our comprehensive study identifies a critical competition between spectrally- and temporally-overlapped guest SE and host PA_p, in which efficient and rapid polaron-pair formation overwhelms SE. Such impulsive polaron-pair formation is prevalent for highly delocalized exciton host materials like PFO, leading to quenching. This does not, however, prevent high steady-state PLQE; efficient polaron-pair recombination and FRET to the F8BT guest allows this.

Changing the host to a material like DBPhFCz with high exciton confinement from its bulky non-planar structure and short conjugation length delays PA_p and allows strong guest SE. As a host, DBPhFCz then yields unprecedented F8BT-based optical gain ($g_{max} \approx 90$ cm^{-1}), with low threshold (2.5 nJ pulse^{-1}) yellow-green (540-590 nm) lasing. The generality of this approach is confirmed by the performance of 3F6 and TrFCz, leading again to efficient SE and lasing. Longer conjugation length F6 oligomers, however, are unsuitable with 5F6 and 7F6 showing rapid polaron-pair formation and no F8BT SE. DBPhFCz has a further advantage, namely its thermally stable ($T_g \approx 308$ °C) glassy microstructure that limits phase segregation, reducing scattering losses and maintaining effective FRET. 3F6 conversely tends to crystallize and phase segregate leading to a loss of gain; structural factors also play an important role. In addition, whilst the chemical differences between DBPhFCz and TrFCz yield significant differences in the charge-injection-relevant host HOMO and LUMO levels this barely affects the guest optical gain (see Table 1), allowing a desirable decoupling of electrical and optical properties.

Recent reports on oxygen-enhanced oligo-fluorene-based liquid lasers[35, 36] are intriguing in the light of our results as those authors proposed that triplet quenching is responsible for laser emission enhancement. However, their ΔA spectra closely match PA_p,[28] leaving open an alternative polaron-pair quenching mechanism.

Finally, F8BT-related materials continue to be of strong interest for electrically pumped light emission structures[31, 32, 41-44] including LEDs and LETs and it will be interesting to explore how beneficial the blend structure optimization performed here for SE and lasing might be in that context.

4. Experimental Section

The novel blue emission host materials DBPhFCz and TrFCz were synthesized in Nanjing University of Posts and Telecommunications following the procedures described in Ref. 4. The PFO host and F8BT guest polymers were supplied by Xi'an Polymer Light Technology Corporation and were used as received. The F8BT molecular weights were M_w = 100,000-150,000 and M_n = 40,000-60,000 and for PFO M_w = 60,000-80,000 and M_n = 15,000-25,000. Fluorene oligomers 3F6 (Mw = 1167), 5F6 (Mw = 1664) and 7F6 (Mw = 2328) were purchased from American Dye Source and used as received. Stock solutions were made up in chloroform (15 mg ml^{-1} for F8BT, 25 mg ml^{-1} for DBPhFCz and 20 mg ml^{-1} for PFO) and used to prepare single component films or mixed in the required ratios to obtain 1 to 75 wt.% F8BT solutions that were used to prepare blend films. Thin film samples for absorption, PL, PL decay, PLQE, pump-probe and ASE measurements were prepared by spin-coating the chloroform solutions onto pre-cleaned synthetic quartz (Spectrosil B) substrates. The thicknesses, *d*, of the F8BT and DBPhFCz:F8BT blend films were fixed at *d* = 180 nm. For DBPhFCz and PFO single component films *d* = 100 nm was used and for PFO:F8BT blend films *d* = 200 nm was used, in all cases thicker than the waveguiding cut-off required for ASE.

UV-vis absorption and PL spectra were recorded using Shimadzu UV-3150 and RF-5300PC spectrometers, respectively. The PLQE of films was measured using an integrating sphere attachment. The transient spectroscopy set-up consisted of a femtosecond Clark MXR regenerative amplifier as primary source delivering 120 fs pulses at 775 nm and 1 KHz repetition rate. The primary beam was split into two. One part was frequency doubled to 387 nm in a β-BaB_2O_4 (BBO) crystal and used as the pump beam. Subsequently, it was sent into a computer controlled delay line before being focused onto the sample to yield ~1 mJ cm^{-2} excitation energy flux. The other beam was in turn focused into a sapphire plate to generate a super continuum probe and was spatially overlapped with the pump spot on the sample. A

spectrometer equipped with a double array optical multichannel detector (Entwicklungsbuero Stresing) operating in single shot acquisition mode was employed to monitor both the transmitted light through the sample and a split-off fraction of the probe as reference. Using a reference channel allows us to record the absorption spectrum for each laser shot, thus monitoring the differences in absorbance upon two consecutive pump-on pump-off acquisitions. This approach reduces to half the number of laser pump shots to which the sample is exposed. Measurements were carried out *in vacuo* to reduce any tendency for photo-oxidation.

For ASE measurements, film (slab waveguide) samples were optically pumped with a Q-switched, neodymium ion doped yttrium aluminium garnate (Nd^{3+}:YAG) laser pumped, type-II BBO, optical parametric oscillator that delivered 5 ns pulses at a repetition rate of 10 Hz. Calibrated neutral density filters were inserted into the beam path to adjust pulse energy incident on the sample. In ASE measurements, an adjustable slit and a cylindrical lens were combined to create a narrow excitation stripe (the pump areas were 550 μm x 4 mm for λ = 370 nm and 700 μm x 4 mm for λ = 450 nm excitation) aligned to the edge of the film sample. The resulting edge emission was collected with a fiber-coupled grating spectrometer equipped with a CCD detector. At sufficient excitation intensities, the spontaneously emitted photons that are waveguided along the stripe-shaped gain region are amplified via SE. This process results in most of the light being emitted from the ends of the stripe. Whilst, strictly there is no threshold for ASE, it is common to define E_{th}^{ASE} as the incident pulse energy at which the FWHM linewidth falls to half that of the low excitation intensity PL spectrum. The gain characteristics of the waveguides were measured with the variable stripe length method.[45] The light intensity emitted from the waveguides as a function of excitation stripe length was recorded for a range of different pump energies. In all cases the polymer layer was thick enough to support a propagating mode at the maximum gain wavelength. To calculate the

gain coefficients, we fitted only those subsets of data for which gain saturation was not evident. For corresponding optical mode loss measurements, the output ASE light intensity was measured as a function of the displacement of a fixed pump stripe (2 mm length) away from the sample edge. The loss measurements were performed at pump energy ~ 5 times E_{th} and the data were fitted assuming an exponential dependence on length. To study thermal stability, slab waveguide film samples comprising DBPhFCz, F8BT and a 10 wt.% F8BT:90 wt.% DBPhFCz blend were annealed in ambient atmosphere for 10 minutes at a range of selected temperatures between room temperature and 260 °C (the limit set by the apparatus) before cooling back to room temperature (at 70 °C min^{-1}) for standard stripe-pumped ASE measurements. DFB lasers were fabricated by pre-patterning silica substrates with 1D surface grating structures (grating period Λ =250 nm for DBPhFCz and Λ = 350 nm for DBPhFCz:F8BT blends, fill factor 50 %, etch depth 50 nm) and then spin-coating films of the gain media on top. The DFB lasers were optically pumped with the same source used for ASE measurements, now focused to a circular spot of 180 μm diameter (2.54 x 10^{-4} cm^2), and their emission was recorded using the same detector. Film thicknesses of 53 to 163 nm were used to tune the DBPhFCz and 150 to 230 nm together with blend composition (5, 15 and 60 wt.% F8BT) to tune the DBPhFCz:F8BT blend lasing wavelengths.

Acknowledgements

We thank Drs Marilu Ariu and Martina Pintani for valuable discussions and Mr Lang Chi, Mr Kang Zhang and Miss Yueting Fang for experimental assistance. We acknowledge funding from the Chinese 973 project (grant 2015CB932203), the National Natural Science Foundation of China (Grants 61376023, 21373114 and 21573111), the Priority Academic Program Development Fund of Jiangsu Higher Education Institutions (PAPD), the Graduate Student Innovation Training Project of Jiangsu (grant KYLX15-0843) and the Chinese Scholarship Council (PhD grants 201408320176 and 201608390023). J.C-G acknowledges financial support from the Spanish Ministry of Economy and Competitiveness through projects MAT2014-57652-C2-1-R (LAPSEN) and PCIN-2015-169-C02-01 (MOFSENS) and the Madrid Regional Government through MAD2D project. DDCB acknowledges financial support from the University of Oxford. IMDEA Nanociencia acknowledges support from the 'Severo Ochoa' Programme for Centres of Excellence in R&D (MINECO, Grant SEV-2016-0686).

References:

[1] F. Hide, M. A. Diaz-Garcia, B. J. Schwartz, M. R. Andersson, Q. B. Pei, A. J. Heeger, *Science,* **1996,** *273,* 1833.

[2] R. Xia, C. Cheung, A. Ruseckas, D. Amarasinghe, I. D. W. Samuel, D. D. C. Bradley, *Adv. Mater.* **2007,** *19,* 4054.

[3] Q. Niu, Q. Zhang, W. Xu, Y. Jiang, R. Xia, D. D. C. Bradley, D. Li, X. Wen, *Org. Electron.* **2015,** *18,* 95.

[4] Y. Qian, Q. Wei, G. Del Pozo, M. M. Mróz, L. Lüer, S. Casado, J. Cabanillas-Gonzalez, Q. Zhang, L. Xie, R. Xia, & W. Huang, *Adv. Mater.* **2014,** *26,* 2937.

[5] U. Scherf, S. Riechel, U. Lemmer, R. F. Mahrt, *Current Opinion in Solid State & Materials Science,* **2001**, *5,* 143.

[6] M. D. McGehee, A. J. Heeger, *Adv. Mater.* **2000,** *12,* 1655.

[7] T. Riedl, T. Rabe, H. H. Johannes, W. Kowalsky, J. Wang, T. Weimann, P. Hinze, B. Nehls, T. Farrell, U. Scherf, *Appl. Phys. Lett.* **2006,** *88,* 241116.

[8] A. E. Vasdekis, G. Tsiminis, J. C. Ribierre, L. O'Faolain, T. F. Krauss, G. A. Turnbull, I. D. W. Samuel, *Opt. Express,* **2006,** *14,* 9211.

[9] M. M. Mroz, G. Sforazzini, Y. Zhong, K. S. Wong, H. L. Anderson, G. Lanzani, J. Cabanillas-Gonzalez, *Adv. Mater.* **2013**, *25,* 4347.

[10] S. Klinkhammer, X. Liu, K. Huska, Y. Shen, S. Vanderheiden, S. Valouch, C. Vannahme, S. Braese, T. Mappes, U. Lemmer, *Opt. Express,* **2012,** *20,* 6357.

[11] Y. Yang, G. A. Turnbull, I. D. W. Samuel, *Appl. Phys. Lett.* 2008, *92,* 163306.

[12] G. Tsiminis, Y. Wang, A. L. Kanibolotsky, A. R. Inigo, P. J. Skabara, I. D. W. Samuel, G. A. Turnbull, *Adv. Mater.* **2013,** *25,* 2826.

[13] R. Xia, P. N. Stavrinou, D. D. C. Bradley, Y. Kim, *J. Appl. Phys.* **2012,** *111,* 123107.

[14] S. Perissinotto, M. Garbugli, D. Fazzi, C. Bertarelli, M. Carvelli, A. R. S. Kandada, Z. Yue, K. S. Wong, G. Lanzani, *ChemPhysChem,* **2011,** *12,* 3619.

[15] R. Gupta, M. Stevenson, A. J. Heeger, *J. Appl. Phys.* **2002,** *92,* 4874.

[16] A. Camposeo, E. Mele, L. Persano, D. Pisignano, R. Cingolani, *Opt. Lett.* **2006,** *31*, 1429.

[17] M. U. Hassan, Y.-C. Liu, H. Butt, K. ul Hasan, J.-F. Chang, A. A. Olawoyin, R. H. Friend, *Journal of Polymer Science Part B-Polymer Physics*, **2016**, *54,* 15.

[18] P. J. Brewer, P. A. Lane, J. S. Huang, A. J. DeMello, D. D. C. Bradley, J. C. DeMello, *Physical Review B,* **2005,** *71,* 205209.

[19] J. Hill, S. Y. Heriot, O. Worsfold, T. H. Richardson, A. M. Fox, D. D. C. Bradley, *Synth. Met.* **2003,** *139,* 787.

[20] A. R. Buckley, M. D. Rahn, J. Hill, J. Cabanillas-Gonzalez, A. M. Fox, D. D. C. Bradley, *Chem. Phys. Lett.* **2001,** *339,* 331.

[21] J. Hill, S. Y. Heriot, O. Worsfold, T. H. Richardson, A. M. Fox, D. D. C. Bradley, *Physical Review B,* **2004,** *69,* 024511.

[22] S. Lattante, A. Cretí, M. Lomascolo, M. Anni, *Org. Electron.* **2016,** *29,* 44.

[23] K.-H. Yim, W. J. Doherty, W. R. Salaneck, C. E. Murphy, R. H. Friend, J.-S. Kim, *Nano Lett.* **2010,** *10,* 385.

[24] M. A. Stevens, C. Silva, D. M. Russell, R. H. Friend, *Physical Review B,* **2001,** *63,* 165213.

[25] D. W. McBranch, B. Kraabel, S. Xu, R. S. Kohlman, V. I. Klimov, D. D. C. Bradley, B. R. Hsieh, M. Rubner, *Synth. Met.* **1999,** *101,* 291.

[26] T. Virgili, G. Cerullo, L. Luer, G. Lanzani, C. Gadermaier, D. D. C. Bradley, *Phys. Rev. Lett.* **2003,** *90*, 247402.

[27] T. Virgili, D. Marinotto, G. Lanzani, D. D. C. Bradley, *Appl. Phys. Lett.* **2005,** *86,* 091113.

[28] F. Montilla, A. Ruseckas, I. D. W. Samuel, *Chem. Phys. Lett.* **2013,** *585,* 133.

[29] T. Virgili, D. Marinotto, C. Manzoni, G. Cerullo, G. Lanzani, *Phys. Rev. Lett.* **2005,** *94,* 117402.

[30] O. J. Korovyanko, Z. V. Vardeny, *Chem. Phys. Lett.* **2002,** *356,* 361.

[31] D. Kabra, M. H. Song, B. Wenger, R. H. Friend, H. J. Snaith, *Adv. Mater.* **2008,** *20,* 3447.

[32] M. C. Gwinner, S. Khodabakhsh, M. H. Song, H. Schweizer, H. Giessen, H. Sirringhaus, *Adv. Funct. Mater.* **2009,** *19,* 1360.

[33] D.-Y. Chung, D.-S. Leem, D. D. C. Bradley, A. J. Campbell, *Appl. Phys. Lett.* **2011,** *98,* 103306.

[34] C. Pflumm, C. Karnutsch, R. Boschert, M. Gerken, U. Lemmer, J. deMello, D. D. C. Bradley, *Proc. SPIE*, **2005,** *5937,* 59370X.

[35] L. Zhao, M. Inoue, K. Yoshida, A. S. D. Sandanayaka, J.-H. Kim, J.-C. Ribierre, C. Adachi, *IEEE J. Sel. Top. Quantum Electron.* **2016,** *22,* 26.

[36] A. S. D. Sandanayaka, L. Zhao, D. Pitrat, J.-C. Mulatier, T. Matsushima, C. Andraud, J.-H. Kim, J.-C. Ribierre, C. Adachi, *Appl. Phys. Lett.* **2016,** *108,* 223301.

[37] C. Gadermaier, L. Romaner, T. Piok, E. J. W. List, B. Souharce, U. Scherf, G. Cerullo, G. Lanzani, *Physical Review B,* **2005,** *72,* 045208.

[38] M. M. Mroz, G. Lanzani, T. Virgili, S. O. Mc Donnell, M. J. Frampton, H. L. Anderson, *Physical Review B,* **2009,** *80,* 045111.

[39] T. Virgili, J. Clark, J. Cabanillas-Gonzalez, L. Bazzana, K. C. Vishnubhatla, R. Osellame, R. Ramponi, G. Lanzani, *J. Mater. Chem.* **2010,** *20,* 519.

[40] C. R. Belton, A. L. Kanibolotsky, J. Kirkpatrick, C. Orofino, S. E. T. Elmasly, P. N. Stavrinou, P. J. Skabara, D. D. C. Bradley, *Adv. Funct. Mater.* **2013**, *23,* 2792.

[41] L. Moretti, L. Criante, G. Lanzani, S. De Silvestri, G. Cerullo, F. Scotognella, *J. Phys. Chem. C,* **2015,** *119,* 23632.

[42] D. O'Brien, A. Bleyer, D. G. Lidzey, D. D. C. Bradley, T. Tsutsui, *J. Appl. Phys.* **1997,** *82*, 2662.

[43] H. Kajii, T. Ohtomo, Y. Ohmori, Kyoto, Japan, 6-8 July 2016. 10.1109/AM-FPD.2016.7543694, 290.

[44] M. Athanasiou, R. M. Smith, S. Ghataora, T. Wang, *Scientific Reports,* **2017,** *7,* 39677.

[45] R. D. Xia, G. Heliotis, Y. B. Hou, D. D. C. Bradley, *Org. Electron.* **2003**, *4*, 165.

[46] J. Chappell, D. G. Lidzey, P. C. Jukes, A. M. Higgins, R. L. Thompson, S. O'Connor, I. Grizzi, R. Fletcher, J. O'Brien, M. Geoghegan, & R. A. L. Jones, *Nat. Mater.* **2003,** *2,* 616.

[47] M. Grell, M. Redecker, K. Whitehead, D. D. C. Bradley, M. Inbasekaran, E. P. Woo, & W. Wu, *Liquid Crystals* **1999,** *26***,** 1403.

[48] I. H. M. Van Stokkum, D. S. Larsen, & R. Van Grondelle, *Bioenergetics,* **2004,** *1657,* 82.

Supporting Information

Host exciton confinement for enhanced Förster-transfer-blend gain media yielding highly efficient yellow-green lasers

Qi Zhang[#] Jingguan Liu, Qi Wei, Xiangru Guo, Yan Xu, Ruidong Xia, Linghai Xie, Yan Qian,* Chen Sun, Larry Lüer, Juan Cabanillas-Gonzalez,* Donal D C Bradley,* Wei Huang**

The Supplementary Materials dataset contains the results of a detailed steady-state and ultrafast-time-resolved optical characterization of thin film gain media comprising ground- and excited-state absorption, photoluminescence (PL), amplified spontaneous emission (ASE) and optical gain and loss measurements. Film topography (using atomic force microscopy (AFM) measurements) and thermal stability have also been investigated. Poly(9,9-dioctylfluorene) (PFO), poly(9,9-dioctylfluorene-*co*-benzothiadiazole) (F8BT), 3,6-*bis*(2,7-di([1,1'-biphenyl]-4-yl)-9-phenyl-9H-fluoren-9-yl)-9-octyl-9H–carbazole (DBPhFCz), 9,9,9",9"-tetraoctyl-9'-phenyl-9'-(3-(N-octyl-carbazole))-2,2':7',2"-terfluorene (TrFCz) and three oligo(9,9-dihexylfluorene)s (3F6, 5F6 and 7F6), together with host:guest blends comprising PFO:F8BT DBPhFCz:F8BT, TrFCz:F8BT and nF6:F8BT over a wide F8BT concentration range have been studied. A detailed description of the procedures used to analyse transient absorption spectra is provided and exemplified for DBPhFCz, PFO and F8BT. Time-dependent excited state concentrations and rates for FRET and guest exciton decay are also extracted from fits to the spectral dynamics. The following Table of Contents summarises the information presented:

Table of contents:

§1. Comparison of DBPhFCz and PFO host materials and their blends with F8BT

§1.1 Thin film absorption and photoluminescence spectra for DBPhFCz, DBPhFCz:F8BT, PFO and PFO:F8BT.

§1.2 AFM-measured film topography for DBPhFCz, DBPhFCz:F8BT, PFO and PFO:F8BT

§1.3 Detailed analysis of transient absorption (DA) spectra, including quantitative determination of cross-sections, time-dependent concentrations and decay rates for DBPhFCz, PFO and F8BT thin film samples

§1.3.1 Calculation of absolute excited-state concentrations

§1.4 Calculation of k_{ET} FRET rates and k_{F8BT} decay rates for DBPhFCz:F8BT blend samples

§1.5 Continuous-wave photoinduced absorption spectra for DBPhFCz and PFO, identifying triplet-triplet transitions

§1.6 Time-dependent population of singlet excitons and polaron-pairs in PFO and DBPhFCz

§1.7 Amplified spontaneous emission (ASE) and distributed feedback (DFB) laser study of DBPhFCz and DBPhFCz:F8BT blends

§2. F6 oligomer host materials and their blends with F8BT

§2.1 Thin film absorption, photoluminescence and ASE spectra for 3F6, F8BT and 3F6:F8BT blends together with PLQE, ASE threshold and optical gain and loss data and AFM images for 3F6:F8BT blend films

§2.2 Transient absorption spectra for nF6 oligomers and nF6 oligomer:F8BT blends

§3. TrFCz host and its blends with F8BT

§3.1 Thin film absorption, photoluminescence and ASE spectra for TrFCz, F8BT and TrFCz:F8BT blends together with PLQE, ASE threshold and optical gain and loss data and AFM images for TrFCz:F8BT blend films

§3.2 Transient absorption spectra for TrFCz and TrFCz:F8BT blends

§4. Thermogravimetry and Differential Scanning Calorimetry data for DBPhFCz

§1. Comparison of DBPhFCz and PFO host materials and their blends with F8BT

§1.1 Thin film absorption and photoluminescence spectra for DBPhFCz, DBPhFCz:F8BT, PFO and PFO:F8BT:

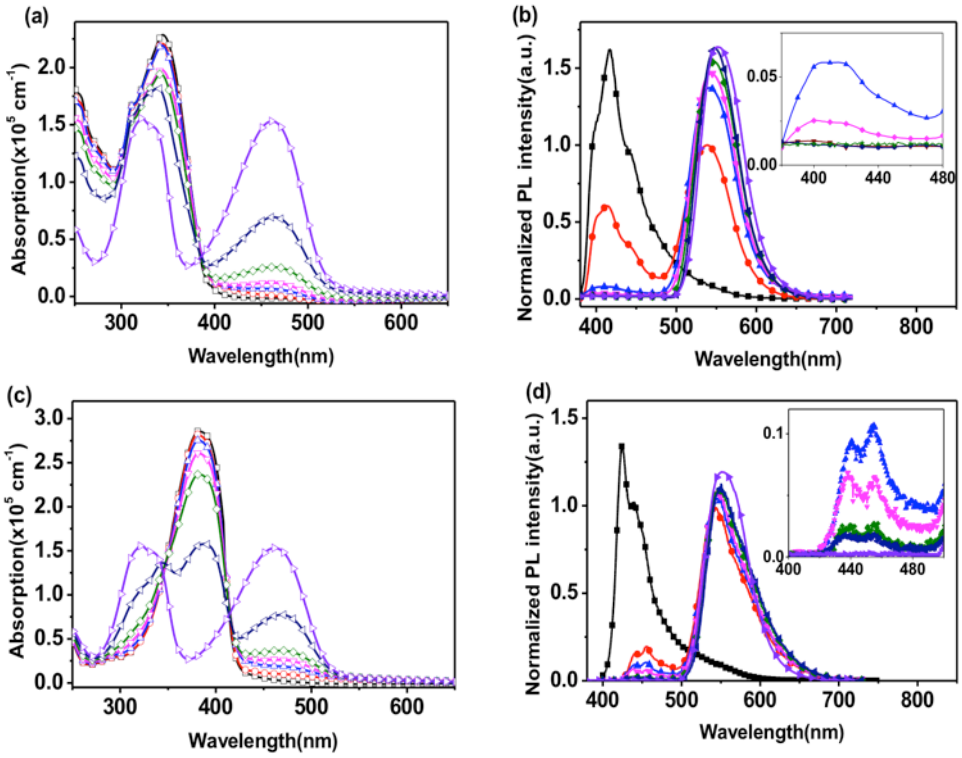

Figure S1: Panels (a) and (b) show the absorption and area-normalized photoluminescence (PL) spectra for 3,6-*bis*(2,7-di([1,1'-biphenyl]-4-yl)-9-phenyl-9H-fluoren-9-yl)-9-octyl-9H–carbazole (DBPhFCz), poly(9,9-dioctylfluorene-*co*-benzothiadiazole) (F8BT) and their blends. (a) From top to bottom at 460 nm the absorption spectra (open symbols) are for F8BT (right triangle), for 50 (left triangle), 20 (diamond), 10 (down triangle), 5 (up triangle) and 1 (circle) wt.% F8BT fraction blends and for DBPhFCz (square). (b) From top to bottom at 420 nm the PL spectra (filled symbols) are for DBPhFCz (square), for 1 (circle), 5 (up triangle), 10 (down triangle), 20 (diamond) and 50 (left triangle) wt.% F8BT blends and for F8BT (right triangle). The inset in (b) shows the short wavelength (DBPhFCz) spectral region for F8BT and ≥ 5wt.% F8BT fraction blend samples on a magnified scale. Panels (c) and (d) show corresponding absorption and PL spectra for poly(9,9-dioctylfluorene) (PFO), F8BT and their blends. (c) From top to bottom at 460 nm the absorption spectra (open symbols) are for F8BT (right triangle), for 50 (left triangle), 20 (diamond), 10 (down triangle), 5 (up triangle) and 1 (circle) wt.% F8BT fraction blends and for PFO (square). (d) From top to bottom at 420 nm the PL spectra (filled symbols) are for PFO (square), for 1 (circle), 5 (up triangle), 10 (down triangle), 20 (diamond) and 50 (left triangle) wt.% F8BT blends and for F8BT (right triangle). The inset in (d) shows the short wavelength (PFO) spectral region for F8BT and ≥ 1wt.% F8BT fraction blend samples on a magnified scale. Both sets of blend absorption spectra can be decomposed into suitably weighted linear superpositions of their component spectra. FRET, however, is more efficient at low (≤ 1 wt.%) F8BT fractions for the PFO blends but less so at higher fractions (≥ 20%) where DBPhFCz blends show greater quenching of host emission. Blend microstructure and host exciton mobility will play an important role in this behavior.

§1.2 AFM-measured film topography for DBPhFCz, DBPhFCz:F8BT, PFO and PFO:F8BT:

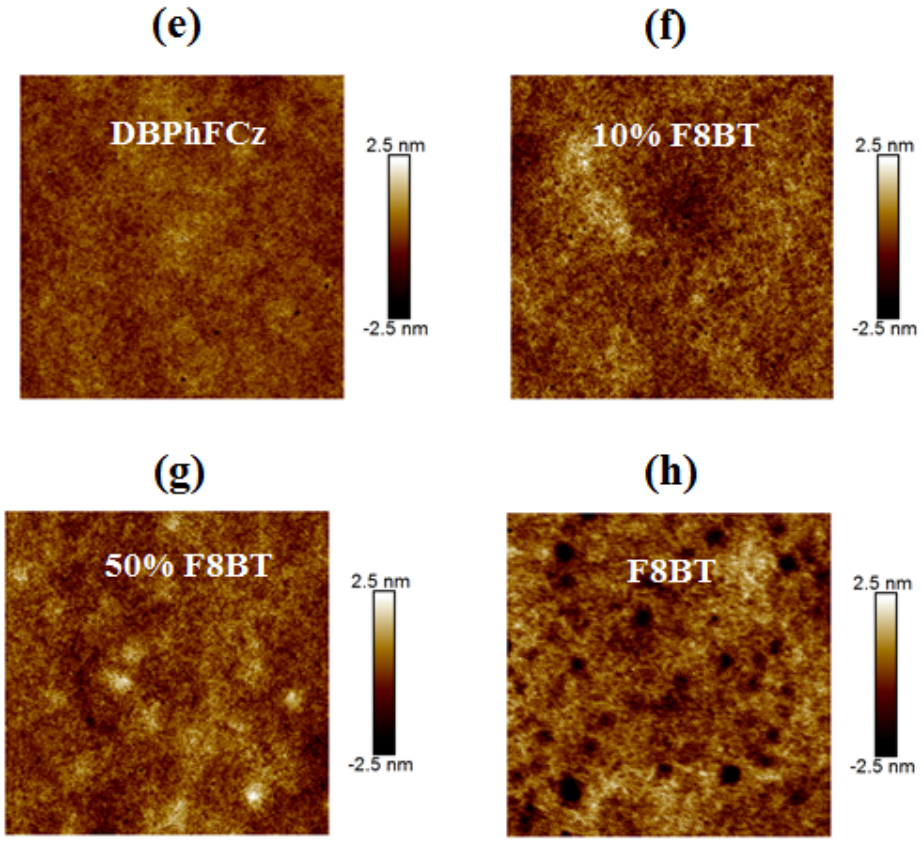

Figure S1 (continued): Panels (e), (f), (g) and (h) show AFM images of DBPhFCz, 10 and 50 wt. % F8BT fraction blend and F8BT thin film samples, respectively, with same height scales (-2.5 to 2.5 nm). The size of the images are 3µm X 3µm.The AFM images are suggestive of an effective host:guest mixing without significant phase separation. Root Mean Square Roughness of DBPhFCz, 10 and 50 wt. % F8BT fraction blend and F8BT thin film is 0.3 nm, 0.5 nm, 0.7 nm and 0.9 nm, respectively.

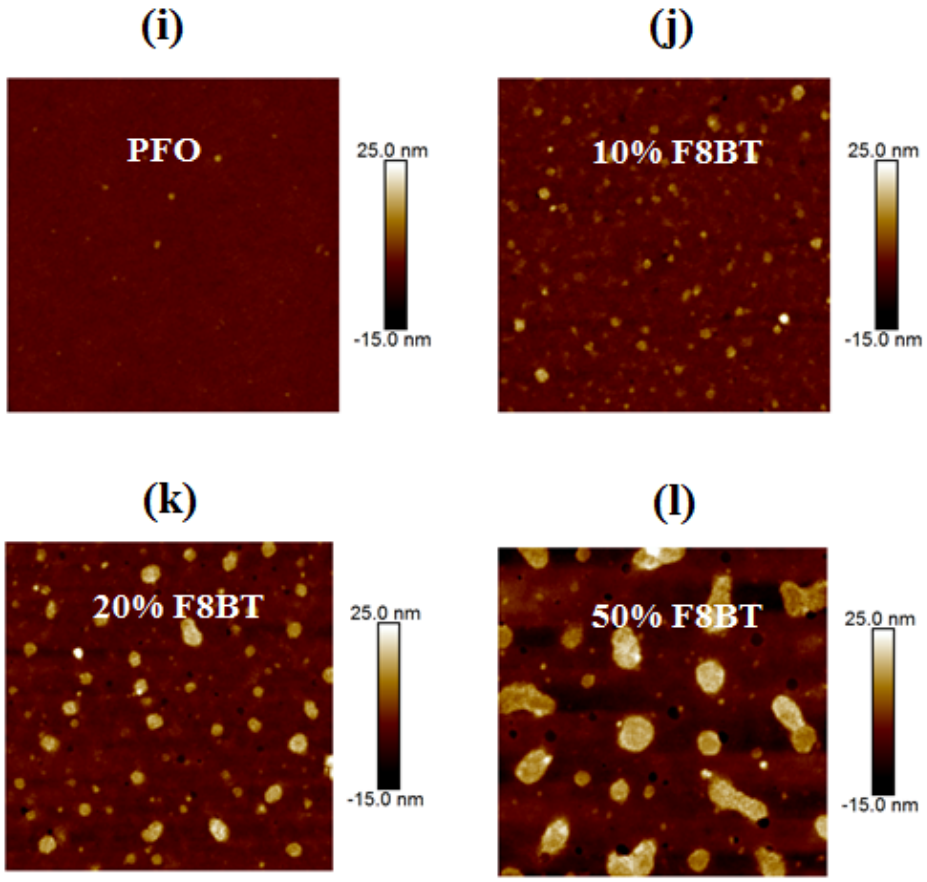

Figure S1 (continued): Panels (i), (j), (k) and (l) show AFM images of PFO and 10, 20 and 50 wt. % F8BT fraction blend thin film samples, respectively, with the same height scales (-15 nm to 25 nm). The size of the images are 3µm X 3µm. Increasing phase separation can be observed as the fraction of F8BT increases. Root Mean Square Roughness of PFO and 10, 20 and 50 wt. % F8BT fraction blend thin film is 0.7 nm, 2.1 nm, 3.7 nm and 6.4 nm, respectively. The images indicate a greater tendency to phase separate than for DBPhFCz:F8BT blends. This does not prevent effective FRET (see panel (d) above), confirming that as previously reported the separated phases are not pure host/guest but rather majority host/guest.[46] It is, however, consistent with residual PFO host emission even at high guest fractions (see panel (d) above).

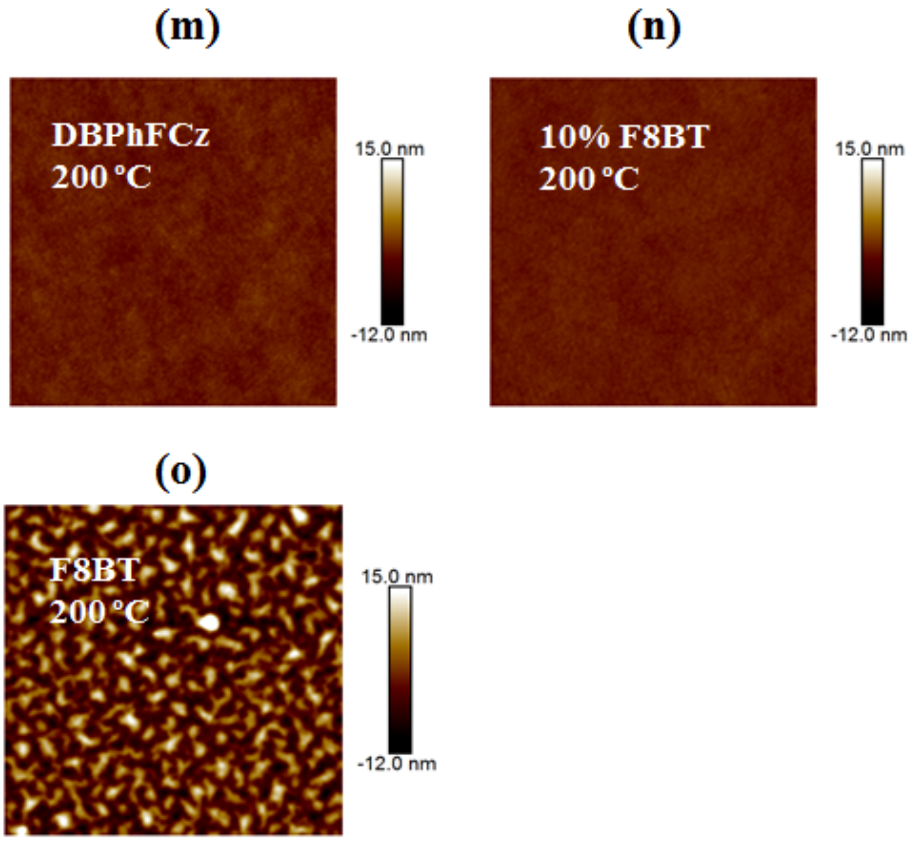

Figure S1 (continued): Panels (m), (n) and (o) show AFM images of DBPhFCz, a 10 wt.% F8BT fraction blend and F8BT, respectively, following annealing at 200°C. The size of the images for DBPhFCz and 10 wt.% F8BT fraction blend are 3µm X 3µm, while the one for F8BT is 10µm X 10µm. Since we intend to show the crystallization in large-scale area. DBPhFCz and the blend show an enhanced roughness (0.3 nm and 0.7 nm, respectively) c.f. non-annealed samples (see panels (e) and (f)) but are otherwise largely unchanged. The F8BT film, however, shows substantial structural rearrangement with considerable roughening (RMS roughness=5.0 nm), consistent with an expected crystallisation above the glass transition temperature, T_g = 130 °C.[47]

§1.3 Detailed analysis of transient absorption (ΔA) spectra, including quantitative determination of cross-sections, time-dependent concentrations and decay rates for DBPhFCz, PFO and F8BT thin film samples:

Transient absorption spectra were analyzed in order to obtain the singlet exciton and polaron-pair densities photogenerated in the host (DBPhFCz and PFO) and guest (F8BT) materials. Doing so as a function of time is not straightforward owing to severe spectral congestion with particularly large overlap between guest singlet exciton stimulated emission (*SE*) and host polaron-pair photoinduced absorption (PA_p); no probe energy could be found that is unique to any one of these excited state transitions. A global fit analysis as previously described in detail by van Stokkum *et al*,[48] was, therefore, applied. In short, the validity of the Beer Lambert law is assumed (system is far from saturated absorption at all probe energies):

$$A(t,\omega) = \sum_i c_i(t)\sigma_i(\omega) \qquad \text{(Equation S1)}$$

to reproduce the measured transient absorption spectrum $A(t,\omega)$, which depends on time t and angular frequency ω, ($\hbar\omega\,(\mathrm{eV}) = \frac{1243\ eV\ nm}{\lambda}$ with λ the wavelength in nm) , as a superposition of i excited state transitions with characteristic time-resolved concentration $c_i(t)$ and energy-resolved absorption cross-section $\sigma(\omega)$. Equation S1 can be written in matrix form:

$$A = c \times \sigma \qquad \text{(Equation S2)}$$

In Equation S2, each column of the c matrix represents one complete concentration-time dependence of a state i, while each row of the σ matrix represents the full (time-invariant) spectrum of that state i.

In a first step, we use singular value decomposition (SVD) to find out the number of states that need to be considered in Equation S2. As Figure S2 shows, DBPhFCz and PFO pump-probe matrices can be reconstructed using two singular values associated with two different

photoexcited states. In line with previous findings in polyfluorenes at these short timescales, we ascribe these two excited states to singlet excitons and polaron-pairs. The spectral shapes σ in equation S2 for the singlet excitons and polaron-pairs were found iteratively by tuning appropriate lineshape functions (Voigt profiles to account for inhomogeneous broadening or skewed Gaussians to account for a Boltzmann type occupation of available states). The cross-sections were reconstructed taking into account the different ingredients composing the spectra of each excited state (photobleach + SE + excited state absorption (PA_s) in the case of singlet excitons and photobleaching + PA_p for polaron - pairs). For the SE and photobleaching bands, we input as initial central energies and full-width-half-maximum (FWHM) linewidths those corresponding to photoluminescence and ground-state absorption, respectively. Initial values for PA_s and PA_p were taken from preliminary reports (in the case of PFO) or estimated from the temporal evolution of ΔA spectra at different times (as in the case of DBPhFCz). The lineshape functions were considered as convergent if they fitted a complete set of twenty spectra at different times across the whole temporal window (0.5 ps-400 ps) and at two different pump intensities, (see Figure S2). F8BT required instead only one cross-section associated to singlet excitons (composed of photobleach + SE + PA_s) to reproduce each spectrum with reasonable agreement. False-colour, wavelength-*vs*-time, ΔA-intensity-height maps are shown in Figure S3 together with reconstructed and difference residual plots that confirm good agreement between measured and fitted data.

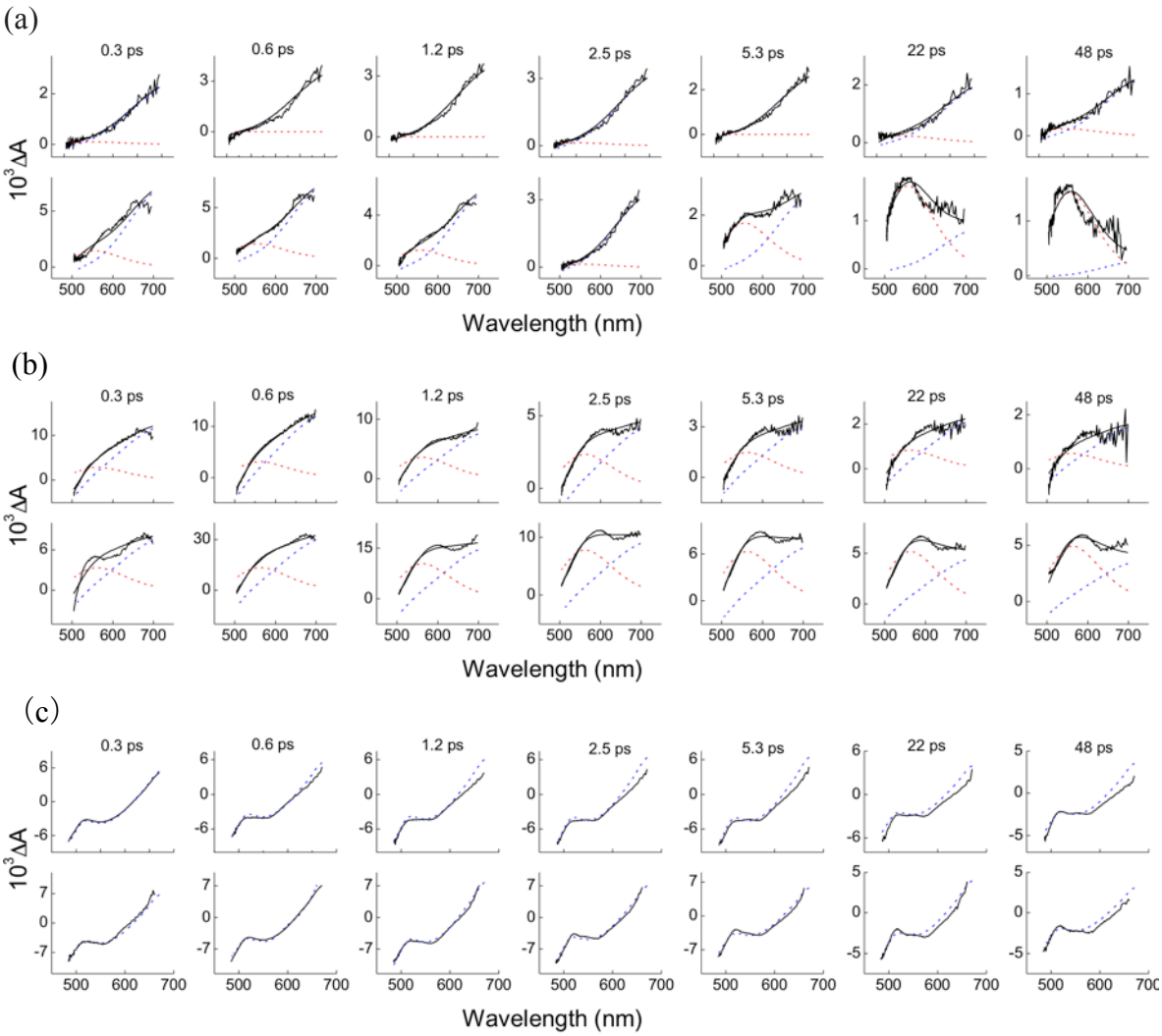

Figure S2: (From top to bottom) (a) ΔA spectra of DBPhFCz at a sequence of early times (0.3 to 48 ps) and pumped with 80 nJ (first row) and 400 nJ (second row) pulse energy. Spectral fits (bold line) to a combination of singlet exciton (blue dashed line) and polaron-pair (red dashed line) weighted components are also shown. (b) Corresponding ΔA spectra for PFO (at same times), again for 80 nJ (third row) and 400 nJ (fourth row) pump pulse energy, together with spectral fits (bold lines) and singlet exciton (dashed blue lines) and polaron-pair (dashed red) components. (c) Corresponding ΔA spectra for F8BT (at same times), with 80 nJ (fifth row) and 400 nJ (sixth row) excitation pulse energy. Fits need only consider a singlet exciton contribution (dashed blue lines) in this case.

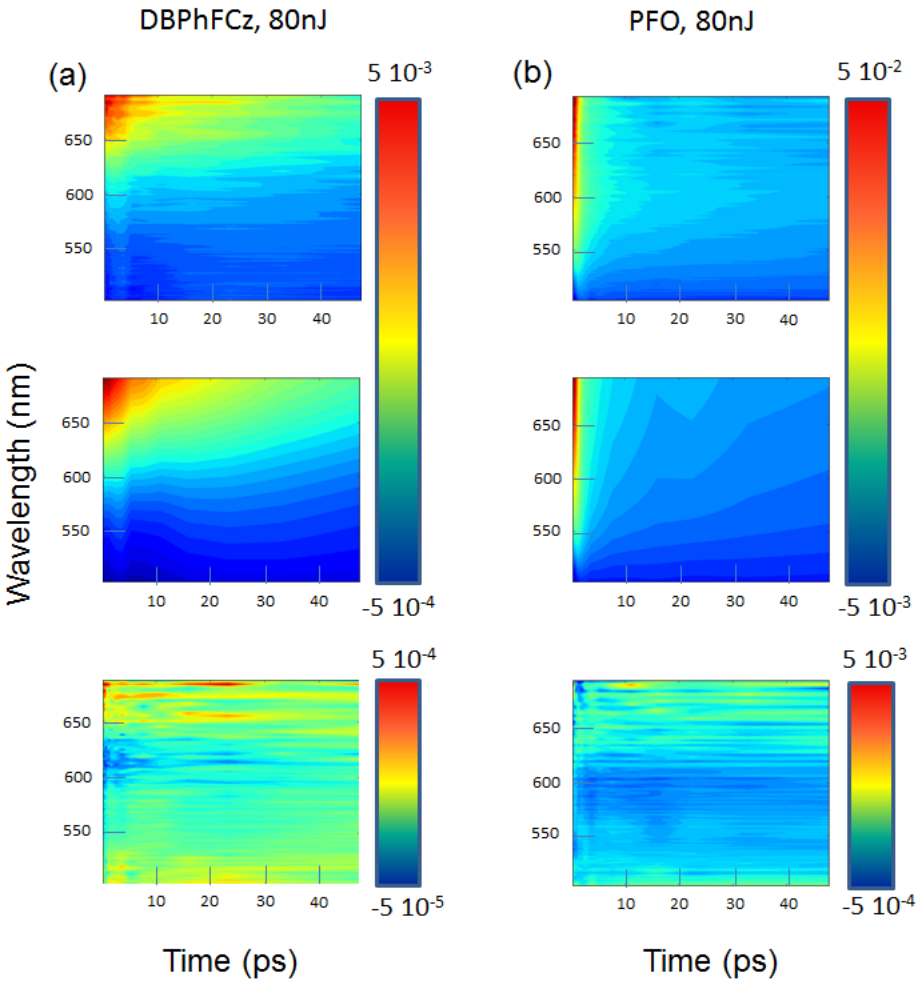

Figure S3: (a) ΔA matrix (top), reconstructed matrix (middle) and residuals (bottom) of DBPhFCz at 80 nJ pump intensity. (b) ΔA matrix (top), reconstructed matrix (middle) and residuals (bottom) of PFO at 80 nJ pump intensity. The false colour scales range between -5 10^{-4} and 5 10^{-3} for DBPhFCz pump-probe and global fit matrices and between -5 10^{-3} and 5 10^{-2} for PFO pump-probe and global fit matrices respectively.

§1.3.1 Calculation of absolute excited-state concentrations:

The spectral modeling, as described above, yields time-resolved spectral weights, which are the areas under the curves associated to each excited state, i, considered in the spectral model:

$$a_i(t) = \int_\omega A_i(\omega, t) d\omega \qquad \text{(Equation S3)}$$

where $A_i(\omega,t)$ is the area underneath the transient absorption spectrum of the i-th excited state and ω stands for the angular frequency, (energy divided by ħ). We can use the spectral weights to calculate the time-resolved concentrations of all excited states present in the system. To this end we combine equation S1 and equation S3:

$$A_i(t, \omega) = d \cdot c_i(t) \cdot \sigma_i(\omega) \qquad \text{(Equation S4)}$$

$$a_i(t) = \int_\omega A_i(t, \omega) d\omega = d \cdot c_i(t) \cdot \int_\omega \sigma_i(\omega) d\omega \qquad \text{(Equation S5)}$$

such that the time-resolved concentration of the i-th photoexcited state is:

$$c_i(t) = \frac{\int_\omega A_i(t,\omega) d\omega}{d \cdot \int_\omega \sigma_i(\omega) d\omega} \qquad \text{(Equation S6)}$$

Now, writing

$$\alpha_i = \int_\omega \sigma_i(\omega) d\omega \qquad \text{(Equation S7)}$$

Equation S6 becomes:

$$c_i(t) = \frac{a_i(t)}{d\alpha_i} \qquad \text{(Equation S8)}$$

This expression leads to a series of i-equations and 2 x i unknowns (α_i and c_i). Additionally, in the absence of any relaxation (at t = 0, assuming that there are no relaxation processes that are faster than our instrumental time resolution of about 150 fs), the total concentration must equal the concentration of absorbed photons:

$$c_{tot} = c_{ph} = \frac{1}{d} \sum_i \frac{a_i(0)}{\alpha_i} \qquad \text{(Equation S9)}$$

Here, the concentration of absorbed photons is given by:

$$c_{ph} = \frac{n_{ph}}{d} = \frac{2N_{ph}(1-T)}{Ad} = 2\frac{N_{ph}}{\pi w_{pu}^2 \cdot d} = \frac{2E_{pu}/E_{ph}}{\pi w_{pu}^2 \cdot d} \qquad \text{(Equation S10)}$$

where $n_{\tilde{p}h}$ is the density of absorbed pump photons per unit area at the position of the probe pulse A, N_{ph} is the total number of absorbed photons, T is the transmission of the sample at the deployed pump wavelength assuming no scattering and reflection losses, A is the effective area of the pump spot, assumed to have a Gaussian profile, w_{pu} is the Gaussian spot size of the pump pulse, E_{pu} is the total energy of a single pump pulse, E_{ph} is the energy of a single photon at the wavelength of the pump pulse. The factor 2 in the last fraction comes from the assumption that the probe pulse spot sits in the center of the pump pulse with a spot size $w_{pr} << w_{pu}$. These assumptions are all more or less justified in our experiment. Equation S.10 then allows us to obtain one additional equation for each excitation intensity employed. In our study, two excitation intensity datasets (80 nJ and 400 nJ) were sufficient to obtain the time-dependent concentrations of singlet excitons and polaron-pairs (namely c1 and c2 in equations S9 and S10).

§1.4 Calculation of k_{ET} FRET rates and k_{F8BT} decay rates for DBPhFCz:F8BT blend samples:

Owing to the delayed polaron-pair formation in DBPhFCz and the efficient DBPhFCz to F8BT energy transfer, the pump-probe dynamics in blends where reproduced assuming an interplay of DBPhFCz and F8BT singlet excitons exclusively. The rates of DBPhFCz to F8BT energy transfer and F8BT decay were estimated with global fit analysis assuming sequential chain reaction involving first photoexcitation of DBPhFCz singlet excitons and their subsequent energy transfer to F8BT:

$$\frac{dS_0^{DBPhFCz}}{dt} = -g + k_{ET}S_1^{DBPhFCz} \qquad \text{(Equation S11)}$$

$$\frac{dS_1^{DBPhFCz}}{dt} = g - k_{ET}S_1^{DBPhFCz} \qquad \text{(Equation S12)}$$

$$\frac{dS_1^{F8BT}}{dt} = k_{ET}S_1^{DBPhFCz} - k_{F8BT}S_1^{F8BT} \qquad \text{(Equation S13)}$$

$$\frac{dS_0^{F8BT}}{dt} = -k_{ET}S_1^{DBPhFCz} + k_{F8BT}S_1^{F8BT} \qquad \text{(Equation S14)}$$

where $S_0^{DPh}, S_0^{F8BT}, S_1^{DBPhFCz}$ and S_1^{F8BT} stand for the ground and excited singlet states in DBPhFCz and F8BT and k_{ET}, k_{F8BT} represent the sought-after energy transfer and F8BT singlet exciton decay rates.

§1.5 Continuous-wave photoinduced absorption of DBPhFCz and PFO:

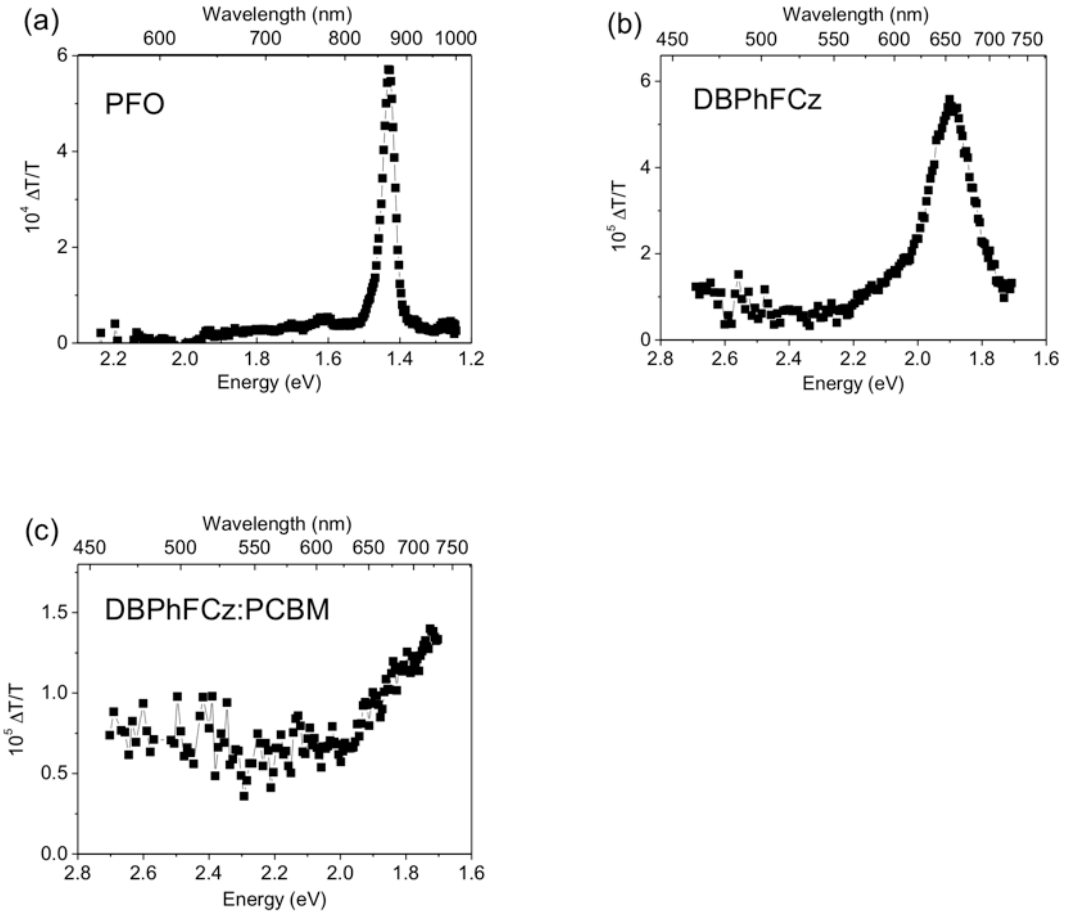

Figure S4: (a) 77K continuous-wave photoinduced absorption (PA) spectra for (a) PFO, (b) DBPhFCz and (c) DBPhFCz:PCBM. The sharp spectral peaks at ≈ 860 nm (1.44 eV) and ≈ 655 nm (1.89 eV) for PFO and DBPhFCz, respectively, correspond to triplet-triplet excited state absorption. Note that such sharp features do not have correspondence with the picosecond TA spectra, confirming the absence of triplet excitons in the timescales relevant for energy transfer and stimulated emission. Likewise, triplet features disappear upon doping DBPhFCz with PCBM, leaving instead a broad spectrum tentatively associated to spectral overlap of DBPhFCz cations and PCBM anions.

§1.6 Time-dependent population of singlet excitons and polaron-pairs in PFO and DBPhFCz:

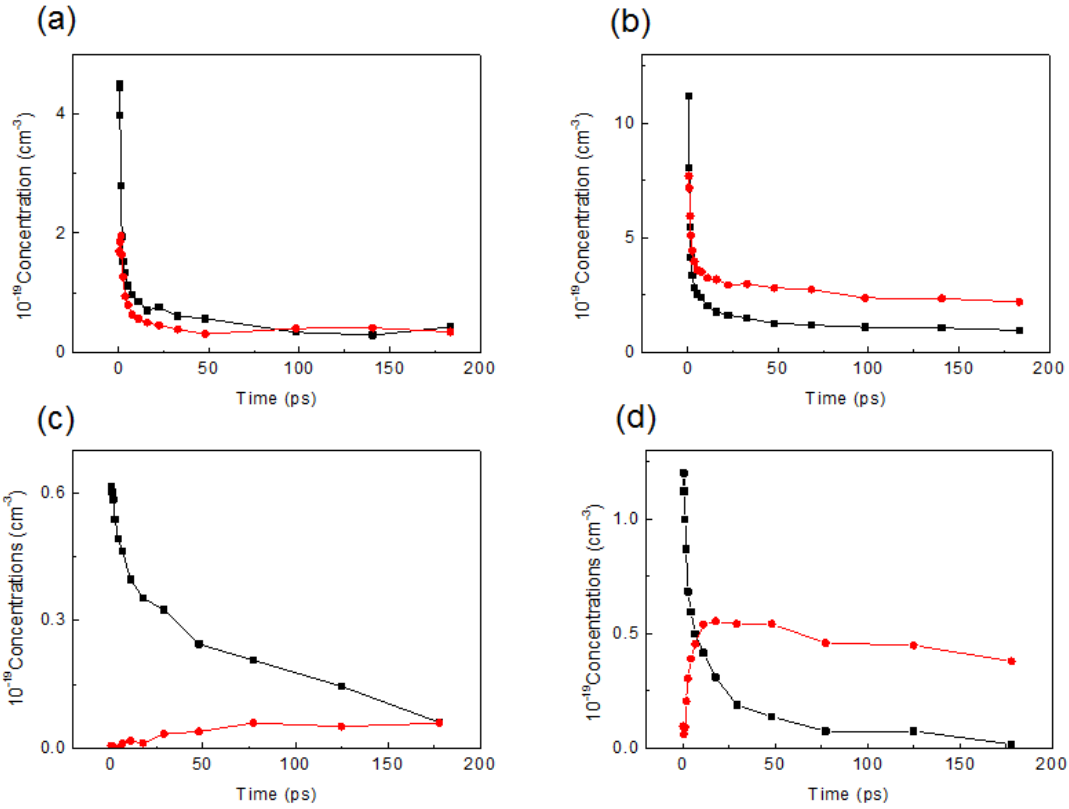

Figure S5: Singlet exciton (black squares) and polaron-pair (red circles) concentrations calculated for PFO at (a) 80 nJ, (b) 400 nJ and for DBPhFCz at (c) 80 nJ and (d) 400 nJ. Note that polaron-pairs have characteristic longer lived components respect to singlet excitons. For DBPhFCz a polaron-pair build-up is observed in contrast with PFO, where polaron photogeneration seems to proceed within the pulse duration.

§1.7 Amplified spontaneous emission (ASE) and distributed feedback (DFB) laser study of DBPhFCz and DBPhFCz:F8BT blends:

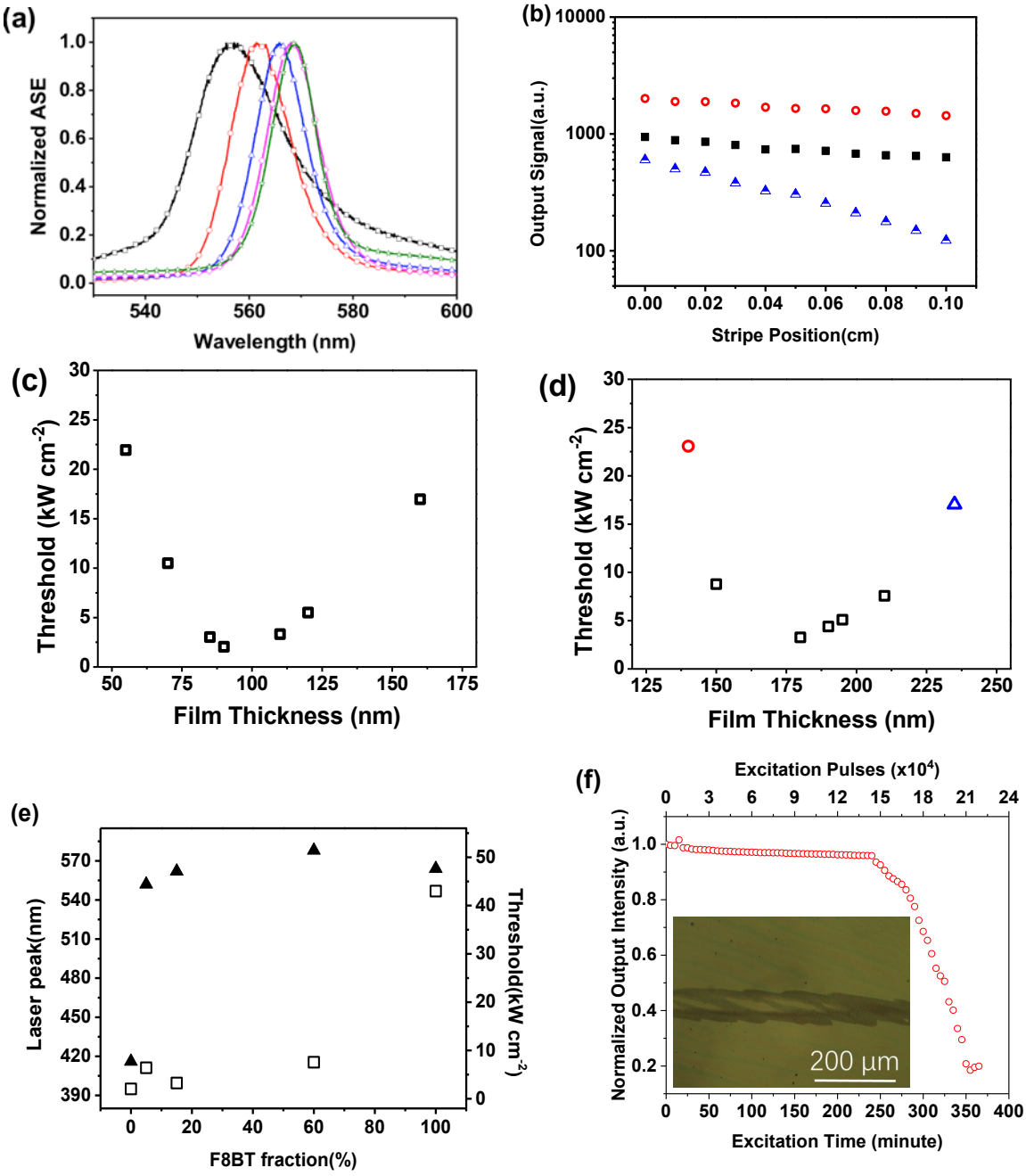

Figure S6: (a) ASE spectra for DBPhFCz:F8BT blends with, from left to right, 5, 15, 30, 50 and 100 wt.% F8BT fraction (film thicknesses 180-200 nm). (b) Stripe displacement propagation data for a 10 wt.% DBPhFCz:F8BT blend film (squares) and for DBPhFCz (circles) and F8BT (triangles) films. The slopes of lines fitted to the data indicate losses of 1.75, 1.39 and 6.76 cm^{-1}, respectively. (c) 1-D, 2nd order DFB laser thresholds (open squares data) for DBPhFCz coated etched silica gratings of period Λ = 250 nm, fill factor 50 % and etch depth 50 nm, plotted as a function of DBPhFCz film thickness.

Figure S6 caption continued: (d) 1-D, 2^{nd} order DFB laser thresholds for DBPhFCz:F8BT blends with 5 (red open circle), 15 (black open squares), and 60 (blue open up-triangle) wt. % F8BT fraction coated on etched silica gratings of period Λ = 350 nm, fill factor 50 % and etch depth 50 nm, plotted as a function of blend film thickness. (e) The lowest achieved DFB laser threshold (open squares, right ordinate) and corresponding laser peak position (filled up-triangles, left ordinate) for blend films as a function of F8BT fraction; data are also shown for DBPhFCz (0% F8BT) and F8BT (100%). (f) ASE output intensity as a function of excitation time for an unencapsulated DBPhFCz:F8BT blend film with 15 wt.% F8BT fraction optical pumped at ~ 8 x $E_{th.}$ After 4 hours continuous pumping with modest decay, the film then suffered more rapid degradation, dropping to 50% output after an additional ~ 85 minutes. Optical damage was clearly visible (see inset microscope image, 50μm scale bar) after 6 hours pumping, by which time the output had fallen to 20%.

§2. F6 Oligomer host materials and their blends with F8BT

§2.1 Thin film absorption, photoluminescence and ASE spectra for 3F6, F8BT and 3F6:F8BT blends together with PLQE, ASE threshold and optical gain and loss data and AFM images for 3F6:F8BT blend films:

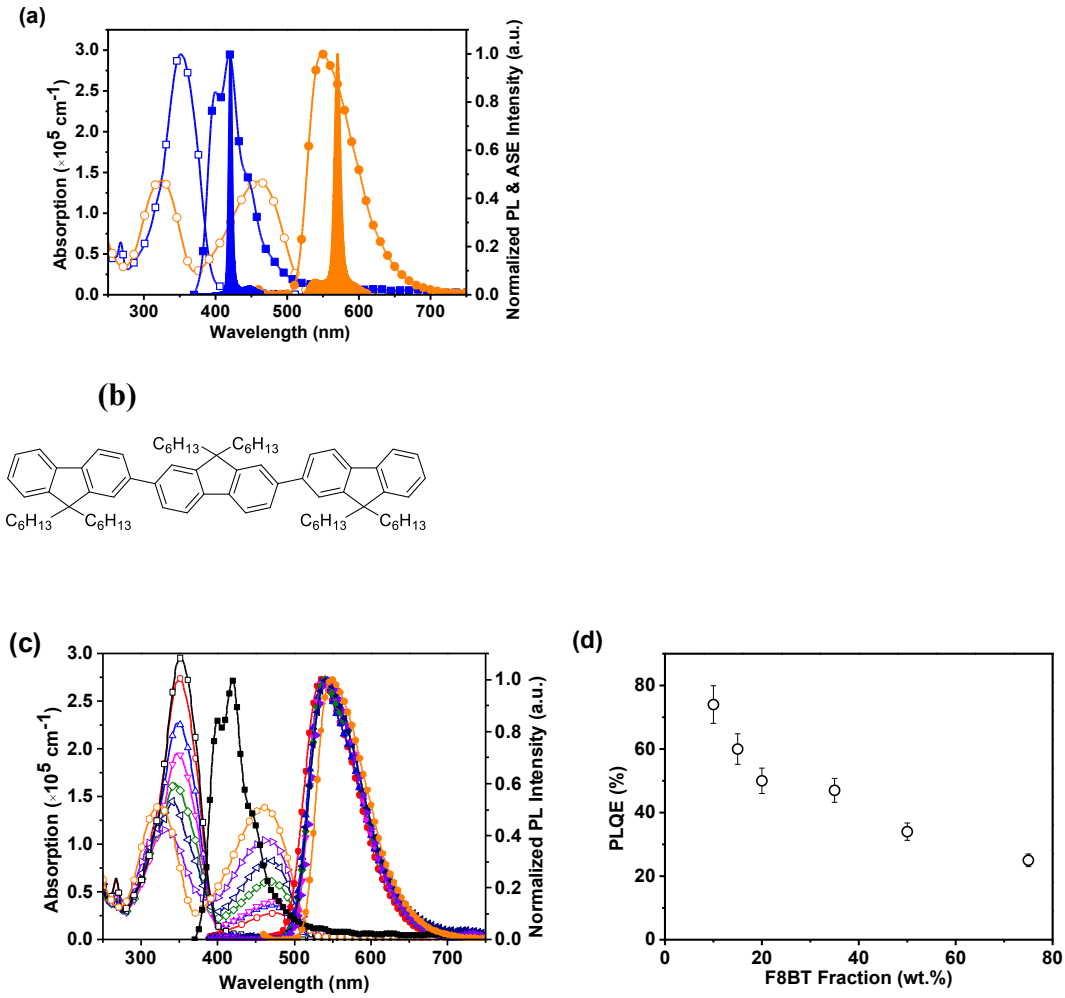

Figure S7. (a) Absorption coefficient (open symbols, left ordinate), PL (filled symbols, right ordinate) and amplified spontaneous emission (ASE) (in-filled) spectra of 3F6 (blue squares and lines) and F8BT (orange circles and lines) thin film samples. (b) Chemical structure of 3F6. (c) Absorption (open symbols) and PL spectra (filled symbols) for 3F6:F8BT blends with different F8BT fractions. Spectra are shown for, from top to bottom in absorption at 350 nm, 0 (black square), 10 (red circle), 15 (blue up triangle), 20 (magenta down triangle), 35 (olive diamond), 50 (navy left triangle), 75 (violet right triangle) and 100 (orange hexagon) wt.% F8BT fractions. (d) PLQE (open circles data) for 3F6:F8BT blends as a function of F8BT fraction.

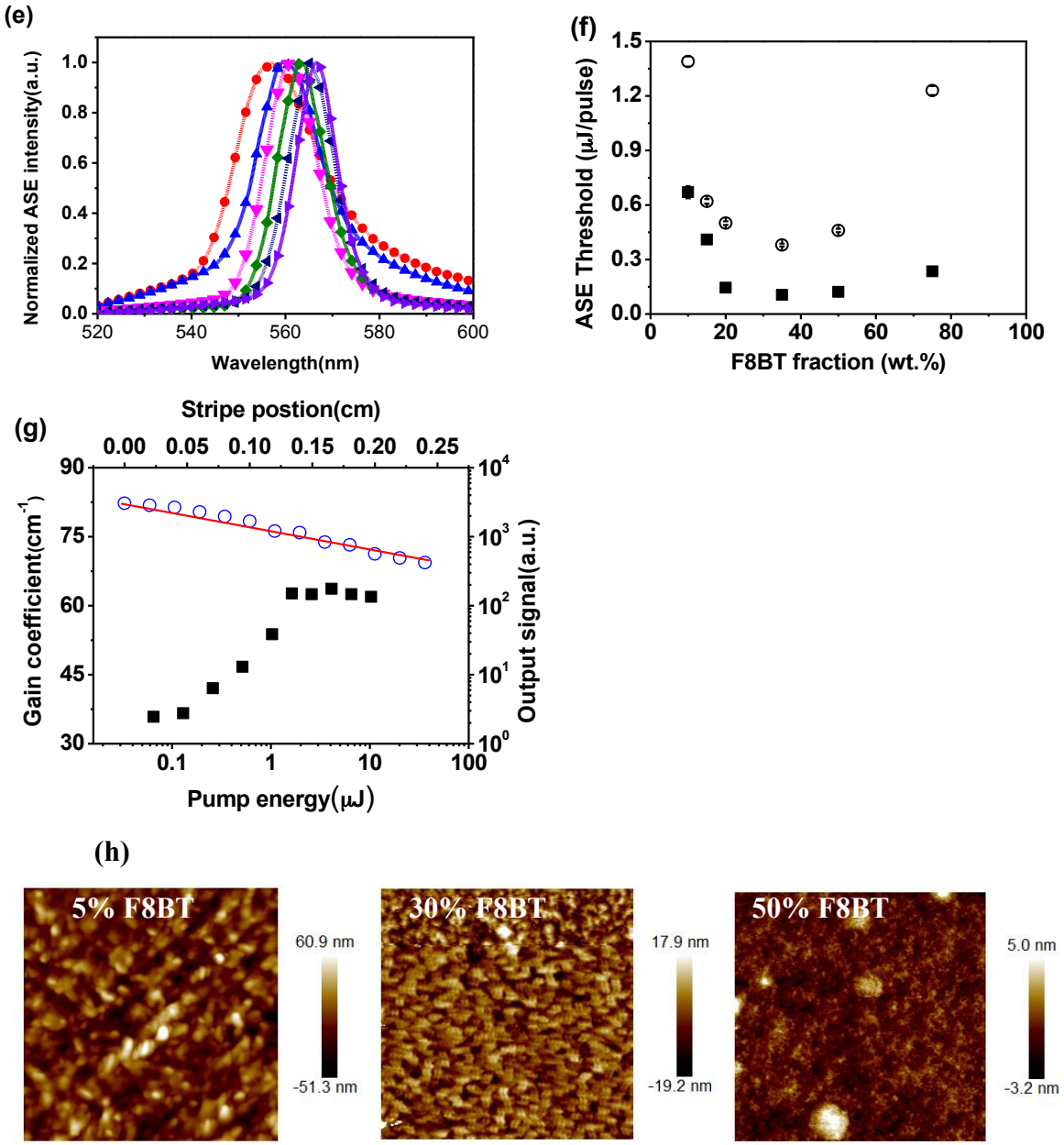

Figure S7 (continued): (e) Typical ASE spectra of 3F6:F8BT blends (film thickness 190-205nm) with, from left to right, 15, 20, 35, 50 and 75 wt.% F8BT fraction. The shifts map the observed shift in PL spectra (panel (c)). (f) ASE thresholds for 3F6:F8BT blends as a function of F8BT concentration with 370 nm (filled squares data) and 450 nm (open circles data) excitation. (g) Gain coefficient (filled squares, left ordinate) as a function of pump energy (lower abscissa) and ASE output signal (open circles with line, right ordinate) as a function of stripe displacement (upper abscissa) for a 35 wt.% F8BT blend sample. The maximum gain is 64 cm^{-1} and the propagation loss deduced from the slope of the stripe displacement curve is 5 cm^{-1}. (h) 10 μm x 10 μm area AFM images for three 3F6:F8BT blend films with different F8BT fractions (5, 30 and 50 wt.% F8BT from left to right).

Table S1: Key parameters for gain-related properties of 3F6:F8BT blend films with different F8BT fractions. α and *PLQE* are the absorption coefficient values at 370 and 450 nm and the photoluminescence quantum efficiency measured for excitation at 370 nm; λ_{ASE} and E_{th}^{ASE} are the ASE peak wavelength and threshold pump energy (defined as the pump pulse energy at which the FWHM linewidth of the emission spectrum halves).

F8BT fraction (wt.%)	10	15	20	35	50	75
α (x 10^5 cm^{-1}) @ λ = 370 nm & 450 nm	1.97 0.23	1.61 0.31	1.36 0.34	1.07 0.53	0.85 0.74	0.53 0.99
PLQE (%)	74	60	50	47	34	25
λ_{ASE} (nm)	557	559.5	561.1	563.4	565.4	566.5
E_{th}^{ASE} (nJ $pulse^{-1}$) pumped@ 370 nm & 450 nm	>670 >1390	510 620	145 500	122 380	105 460	235 1230

§2.2 Transient absorption spectra for nF6 oligomers and nF6 oligomer:F8BT blends

3F6 data:

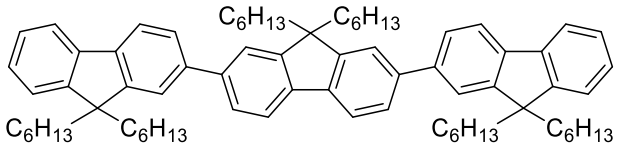

3F6

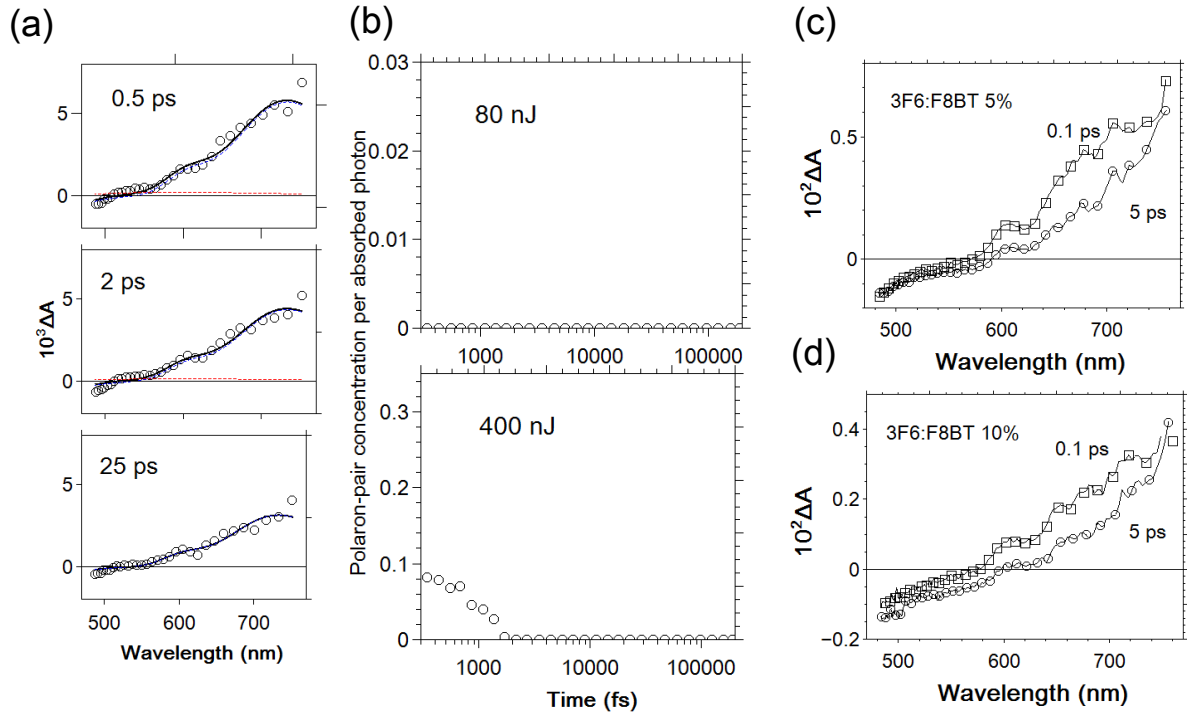

Figure S8: (a) Transient absorption (open circles data) spectra for 3F6 thin film samples at 0.5 ps (upper panel), 2 ps (middle panel) and 25 ps (lower panel) pump-probe delay following excitation with 150 fs pulses (1 kHz) at 387 nm. The black bold lines are fits employing single exciton (dashed blue, predominant component), and polaron-pair (dashed red, negligible amplitude) cross-sections. (b) Time-dependent polaron-pair concentrations deduced (see above for details) for 3F6 at 80 (upper panel) and 400 (lower panel) nJ pump pulse energy. (c) and (d) Transient absorption spectra for 3F6:F8BT blends with 5 (upper panel) and 10 (lower panel) wt.% F8BT concentrations, respectively, at 0.1 and 5 ps pump-probe delay. F8BT SE is evident in the 540 - 565 nm spectral range after 5 ps for the 5% and 10% blends.

5F6 data:

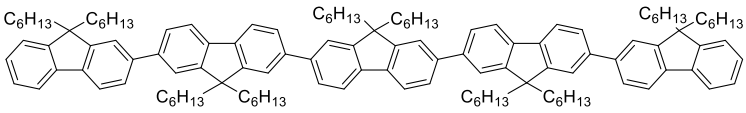

5F6

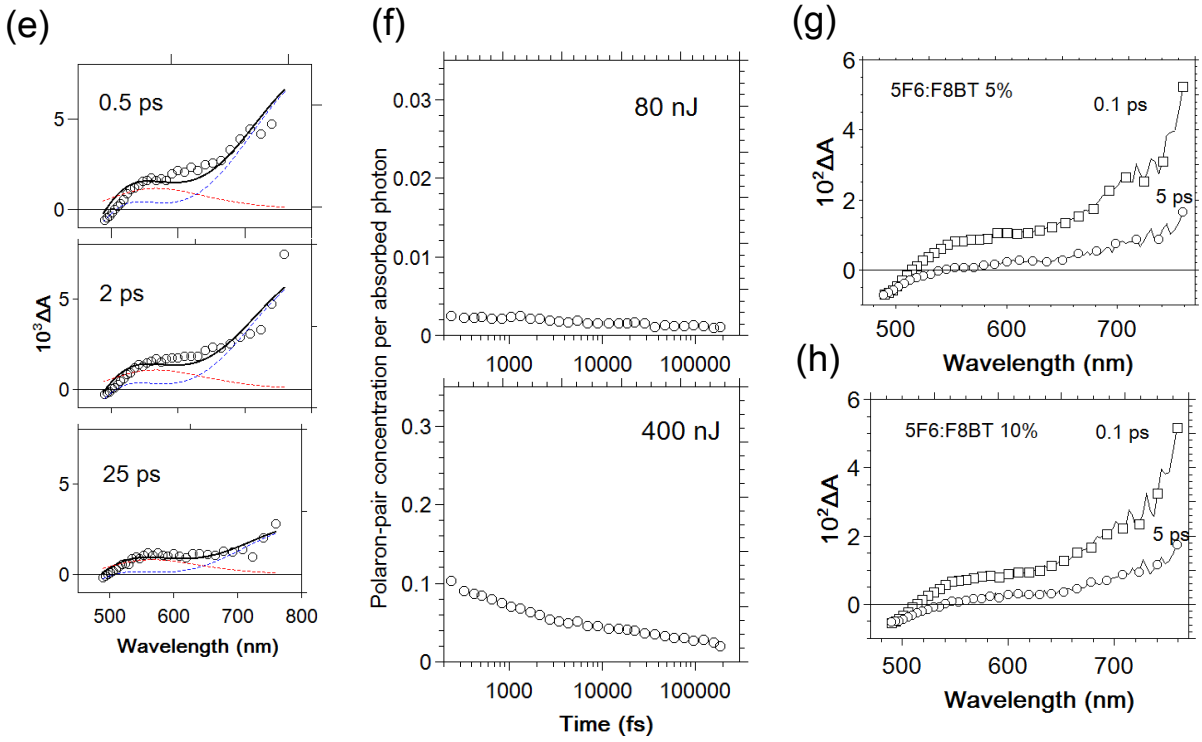

Figure S8 (continued): (e) Transient absorption spectra for 5F6 thin films at 0.5 ps (upper panel), 2 ps (middle panel) and 25 ps (lower panel) pump-probe delay following excitation with 150 fs pulses (1 kHz) at 387 nm. The bold lines are fits employing single exciton (dashed blue) and polaron-pair (dashed red) cross-sections. (f) Time-dependent polaron-pair concentrations for 5F6 at 80 (upper panel) and 400 (lower panel) nJ pump pulse energy. (g) and (h) Transient absorption spectra for 5F6:F8BT blends with 5 (upper panel) and 10 (lower panel) wt.% F8BT concentrations, respectively, at 0.1 and 5 ps pump-probe delay. No F8BT SE is observed.

7F6 data:

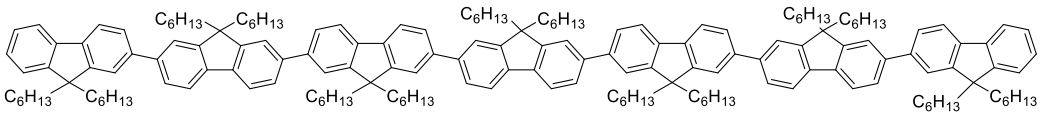

7F6

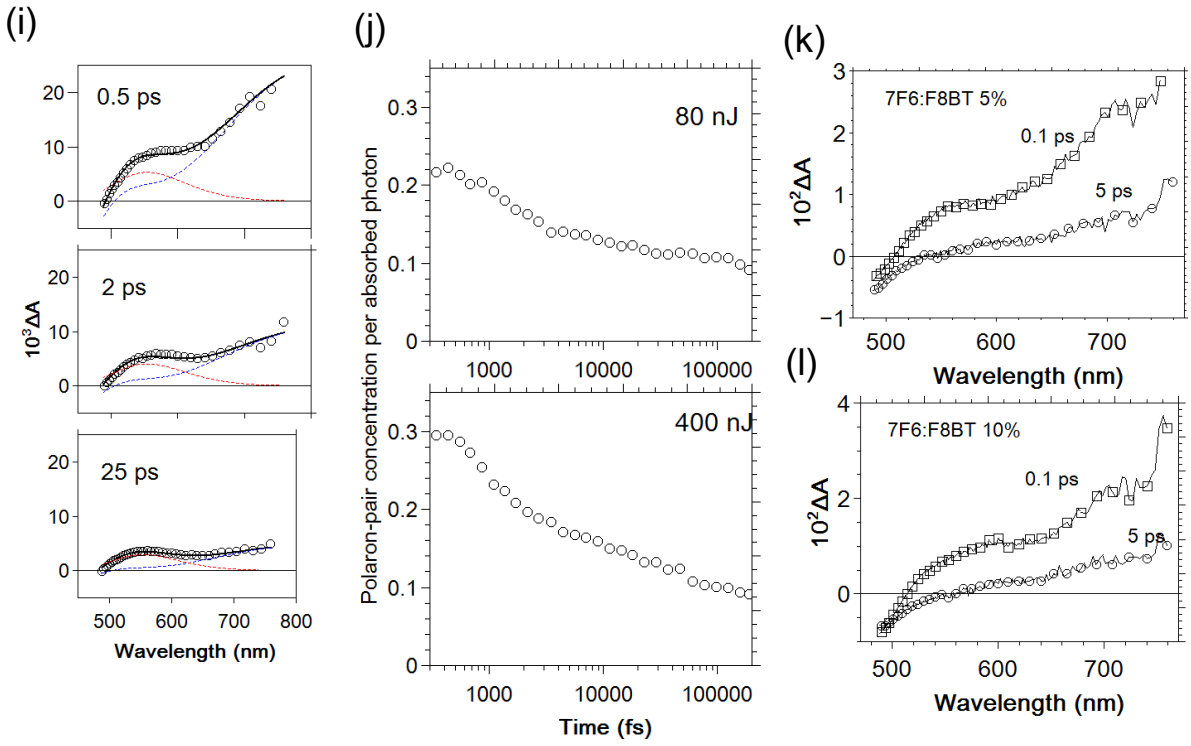

Figure S8 (continued): (i) Transient absorption spectra for 7F6 thin film samples at 0.5 ps (upper panel), 2 ps (middle panel) and 25 ps (lower panel) pump-probe delay following excitation with 150 fs pulses (1 kHz) at 387 nm. The bold lines are fits employing singlet exciton (dashed blue) and polaron-pair (dashed red) cross-sections. (j) Time-dependent polaron-pair concentrations for 7F6 at 80 (upper panel) and 400 (lower panel) nJ pump pulse energy. (k) and (l) Transient absorption spectra for 7F6:F8BT blends with 5 (upper panel) and 10 (lower panel) wt.% F8BT concentrations, respectively, at 0.1 and 5 ps pump-probe delay. No F8BT SE is observed.

§3. TrFCz host and its blends with F8BT

§3.1 Thin film absorption, photoluminescence and ASE spectra for TrFCz, F8BT and TrFCz:F8BT blends together with PLQE, ASE threshold and optical gain and loss data and AFM images for TrFCz:F8BT blend films.

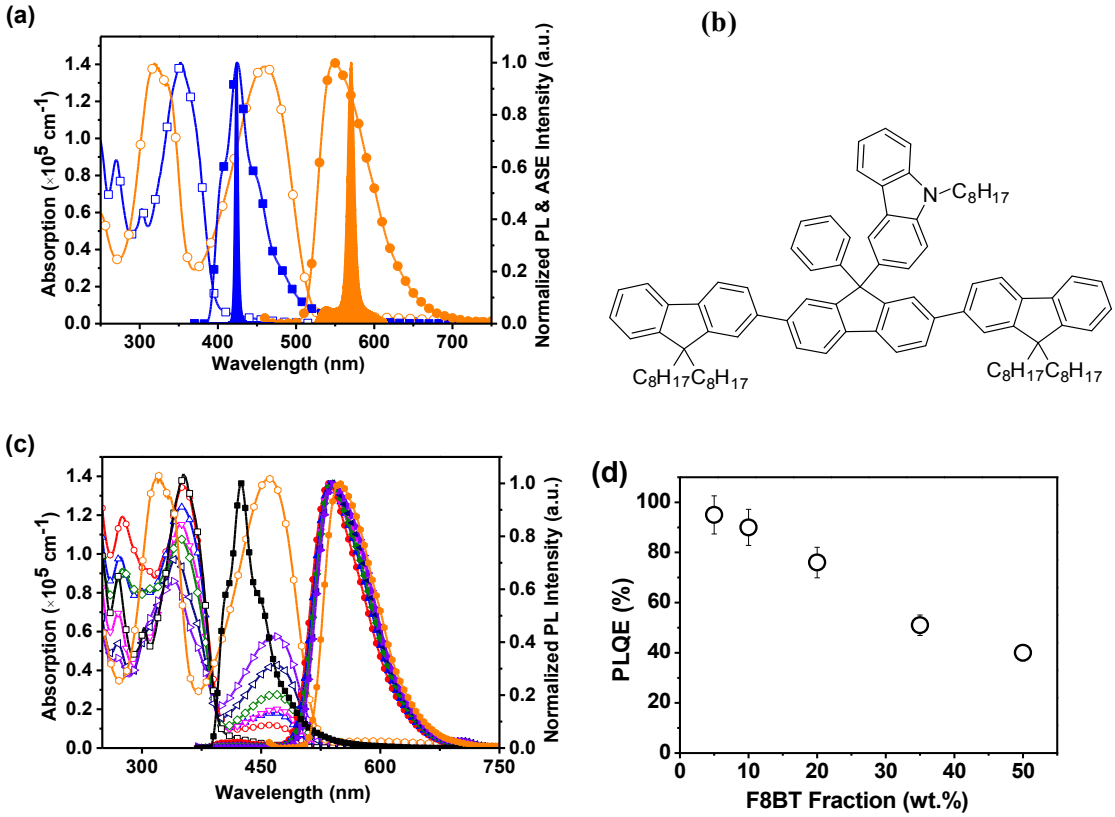

Figure S9: (a) Absorption coefficient (left ordinate, open symbols), photoluminescence (right ordinate, filled symbols) and ASE (right ordinate, in-filled) spectra of TrFCz (blue, squares) and F8BT (orange, circles). (b) Chemical structure of TrFCz (Synthesis details of TrFCz can be found in our previous report).[4] (c) Absorption and PL spectra for TrFCz:F8BT blends with different F8BT fractions. Spectra are shown for, from top to bottom in absorption at 360 nm, 0 (black square), 5 (red circle), 10 (blue up triangle), 15 (magenta down triangle), 20 (olive diamond), 35 (navy left triangle), 50 (violet right triangle) and 100 (orange hexagon) wt.% F8BT fractions. (d) PLQE (open circles data) of TrFCz:F8BT blends as a function of F8BT concentration.

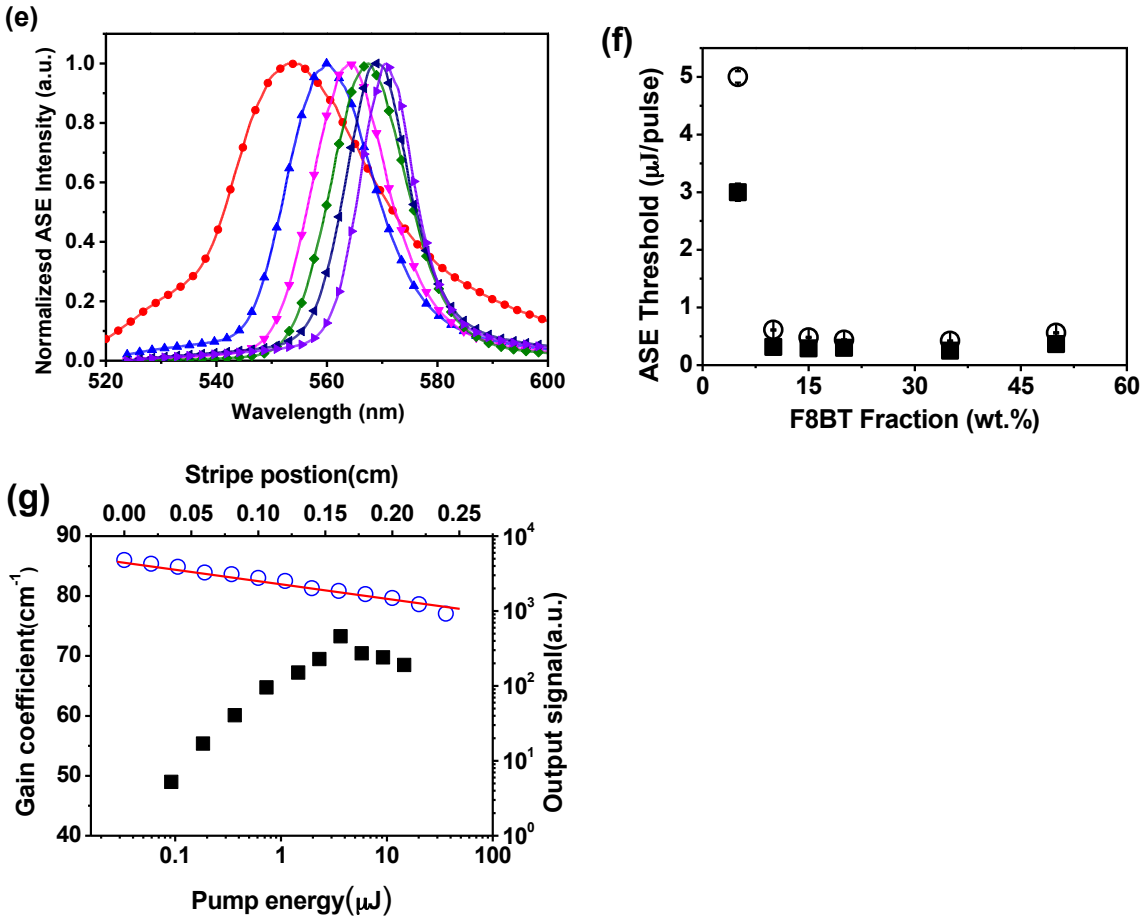

(h)

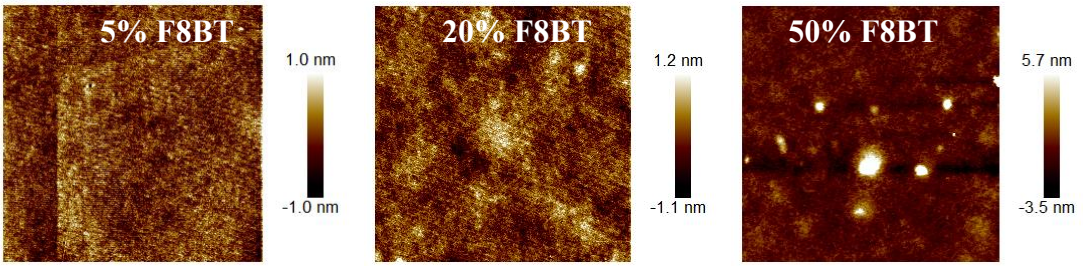

Figure S9 (continued): (e) Typical ASE spectra of TrFCz:F8BT blends with, from left to right, 5, 10, 15, 20, 35 and 50 wt.% F8BT fraction. The shifts map the observed shift in PL spectra (panel (c)). (f) ASE thresholds for TrFCz:F8BT blends (film thickness 190-200nm) as a function of F8BT concentration with 370 nm (filled squares data) and 450 nm (open circles data) excitation. (g) Gain coefficient (filled squares, left ordinate) as a function of pump energy (lower abscissa) and ASE output signal (open circles with line, right ordinate) as a function of stripe displacement (upper abscissa) for a 35 wt.% F8BT blend sample. The maximum gain is 73 cm^{-1} and the propagation loss deduced from the slope of the stripe displacement curve is 6 cm^{-1}. (h) 10 μm x 10 μm area AFM images for three TrFCz:F8BT blend films with different F8BT fractions (5, 30 and 50 wt.% F8BT from left to right).

Table S2. Key parameters for gain-related properties of TrFCz:F8BT blend films with different F8BT fractions. α and *PLQE* are the absorption coefficient values at 370 and 450 nm and the photoluminescence quantum efficiency measured for excitation at 370 nm; λ_{ASE} and E_{th}^{ASE} are the ASE peak wavelength and threshold pump energy **(**defined as the pump pulse energy at which the FWHM linewidth of the emission spectrum halves**).**

F8BT fraction (wt.%)	5	10	15	20	35	50
α (x 10^5 cm^{-1}) @ λ = 370 nm & 450 nm	 1.06 0.11	 1.00 0.16	 0.87 0.17	 0.80 0.25	 0.64 0.38	 0.51 0.52
PLQE (%)	95	90	80	76	51	40
λ_{ASE} (nm)	553-	550	563.5	567	568	570.5
E_{th}^{ASE} (nJ $pulse^{-1}$) pumped@ 370 nm & 450 nm	 >3000 >5000	 315 610	 290 480	 305 440	 250 420	 365 560

§3.2 Transient absorption spectra for TrFCz and TrFCz:F8BT blends.

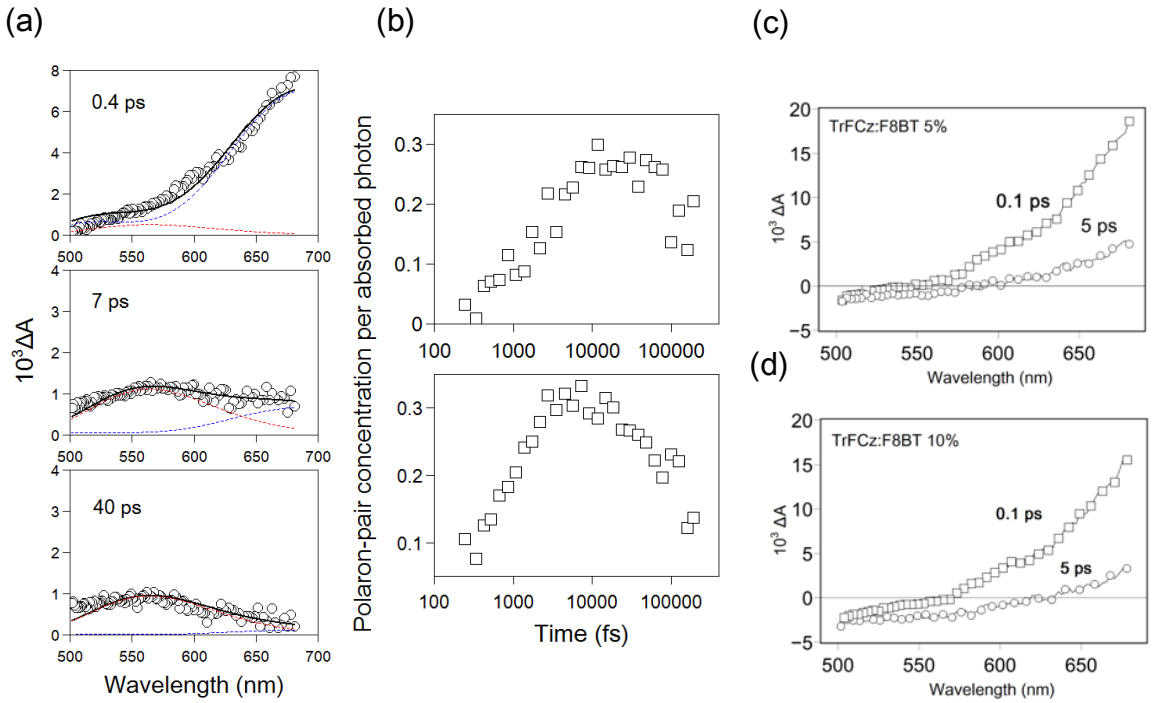

Figure S10: (a) Transient absorption (open circles data) spectra for TrFCz thin film samples at 0.4 ps (upper panel), 7 ps (middle panel) and 40 ps (lower panel) pump-probe delay following excitation with 150 fs pulses (1 kHz) at 387 nm. Fits to singlet exciton (blue dotted line) and polaron-pair (red dotted line) cross-sections are shown together with the overall fit (solid black line). (b) Time-dependent polaron-pair concentrations deduced (see above for details) for TrFCz at 80 (upper panel) and 400 (lower panel) nJ pump pulse energy. The dynamics clearly display a gradual build-up of polaron-pairs, in clear contrast with PFO. (c) and (d) Transient absorption spectra for TrFCz:F8BT blends with 5 (upper panel) and 10 (lower panel) wt.% F8BT, respectively, at 0.1 (open squares data) and ≈ 5 ps (open circles data) pump-probe delay. Unlike the case for PFO:F8BT blends, in TrFCz:F8BT blends F8BT SE (540 - 565 nm spectral range) is evident at 5 ps delay for both 5 and 10 wt. % blends.

§4. Thermogravimetry and Differential Scanning Calorimetry data for DBPhFCz

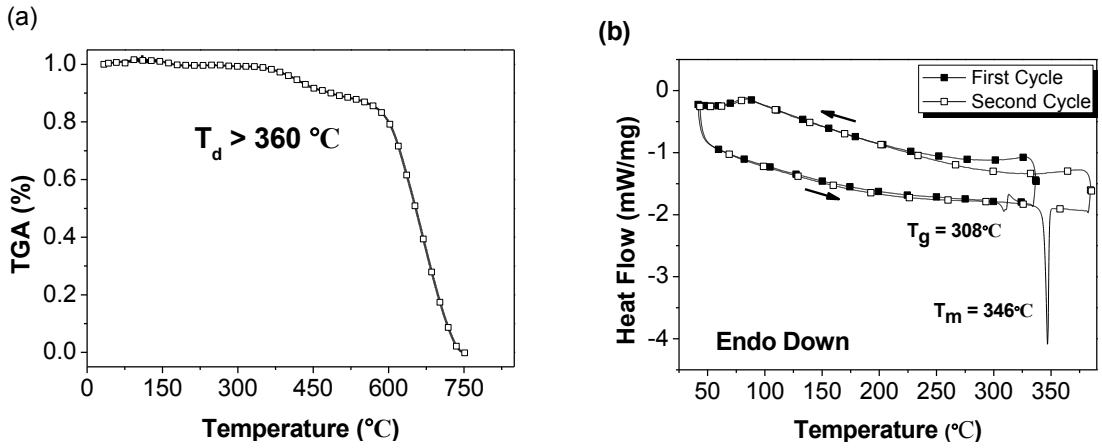

Figure S11: (a) Thermogravimetric analysis (TGA) curve for DBPhFCz displaying a degradation onset temperature above 350 °C. (b) Differential scanning calorimetry curves for DBPhFCz with heating/cooling rates of 10 ^{o}C min^{-1}. A glass transition temperature (T_g) was detected at 308 °C on first heating with a melting transition (T_m) subsequently seen at 346 °C on re-heating. These data confirm that spin-coating DBPhFCz produces glassy films that can be thermally crystallised by heating above T_g.